Palaeogeography, Palaeoclimatology, Palaeoecology 618 (2023) 111525

Contents lists available at ScienceDirect

Palaeogeography, Palaeoclimatology, Palaeoecology

journal homepage: www.elsevier.com/locate/palaeo

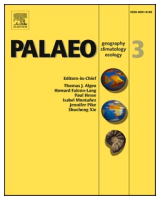

Detection of a mid-Holocene climate event at 7.2 ka BP based on an analysis of globally-distributed multi-proxy records

Mei Hou [a,b], Wenxiang Wu [a,*], David J. Cohen [c], Zhaoqi Zeng [a,b], Han Huang [a], Hongbo Zheng [d], Quansheng Ge [a]

[a] Key Laboratory of Land Surface Pattern and Simulation, Institute of Geographic Sciences and Natural Resources Research, Chinese Academy of Sciences, Beijing 100101, China
[b] University of Chinese Academy of Sciences, Beijing 100049, China
[c] Department of Anthropology, National Taiwan University, Taipei 10617, China
[d] Research Center for Earth System Science, Yunnan University, Kunming 650091, China

ARTICLE INFO

Editor: H Falcon-Lang

Keywords:
7.2 ka event
Summer monsoon
Solar activity
Volcanic eruption

ABSTRACT

Identification of Holocene climate events, their temporal and spatial characteristics, and their causal mechanisms are important for understanding past climate systems with implications for interpreting ancient cultural transformations. In this paper, we analyse globally-distributed, high-resolution climate proxy records from 58 sites to develop a comprehensive understanding of climate change around 7.2 ka BP. Analysis of the data compilation, which comprises records from lake sediments, one loess section, speleothems, marine sediments, and ice cores, show that the climate event is manifested as a weakening of the Asian summer monsoon and a strengthening of the South American summer monsoon. Climate change also involves dramatic cooling and wetter conditions in north-central Europe, widespread aridity across the Africa and west-south North America, contrasting patterns of precipitation variability throughout the Mediterranean, and notable cooling over the polar regions, suggesting that this is a global climate event. A close correspondence between the 7.2 ka event and the timing of solar irradiance minima, strong volcanic eruptions, meltwater flux into the North Atlantic Ocean, and an orbitally-induced decrease in summer solar insolation suggests a possible causal link with these phenomena. We suggest that climate anomalies around 7.2 ka BP may be specifically explained as a response to southward migration of the Intertropical Convergence Zone, onset of an increasingly El Niño-like state, reinforcement of the westerlies, and slowing of the Atlantic Meridional Overturning Circulation (AMOC).

1. Introduction

Future climate change and its potential effects on human society and ecosystems are of prime concern to all. Climate modeling suggests that human-induced forcings are increasing the probability of abrupt climate change in the next hundred years or beyond (National Research Council, 2002; IPCC, 2021). One way to deal with the possible impact of future abrupt climate change is to look to the past for possible close analogs (Alley and Ágústsdóttir, 2005). During the past few decades, especially following the establishment of PAGES (Past Global Changes) in 1991, great advances have been made in the reconstruction of precisely-dated and highly-resolved proxy records. For example, evidence from ice rafted debris (IRD) in the North Atlantic (Bond et al., 1997) and glaciochemical series in a Greenland ice core (O'Brien et al., 1995) revealed that the warm Holocene originally understood through the oxygen isotopes of ice cores (Dansgaard et al., 1993) was unstable and punctuated by several significant climate variations. These climate changes potentially had large and far-reaching consequences on human societies. Furthermore, they typically occurred at times when the background climate was much like the present (Bond et al., 2001; Mayewski et al., 2004; Wang et al., 2005; Shuman, 2012). Therefore, the study of such episodes can provide insights into the processes, drivers, and impacts of abrupt climate change, and these can then be applied to understand the behavior of climate systems and react to the likely occurrence of future abrupt climate change.

Among these past episodes, the 8.2 ka BP event (ka BP = thousand

* Corresponding author at: Key Laboratory of Land Surface Pattern and Simulation, Institute of Geographic Sciences and Natural Resources Research, Chinese Academy of Sciences, 11A, Datun Road, Chaoyang District, Beijing 100101, China.
E-mail address: wuwx@igsnrr.ac.cn (W. Wu).

https://doi.org/10.1016/j.palaeo.2023.111525
Received 30 October 2022; Received in revised form 20 March 2023; Accepted 21 March 2023
Available online 22 March 2023

years before 1950 present) (Alley et al., 1997; Alley and Ágústsdóttir, 2005), 5.5 ka BP event (Brooks, 2006; Wu et al., 2018; Hou and Wu, 2021), and 4.2 ka BP event (Wu and Liu, 2004; Roberts et al., 2011; Weiss, 2016) have received considerably more attention because of their climatic and/or potential past socio-cultural significance. Evidence is emerging to identify other potential Holocene climate events. One such climate event, discussed in this paper, appears to occur approximately 7.6–7.0 ka BP, as indicated by widespread paleoclimate records from the North Atlantic (Bond et al., 2001), Europe (Magny, 2004; Magny et al., 2011), the Mediterranean (Magny et al., 2013; Cheng et al., 2015), Asia (Yu et al., 2004; Gupta et al., 2005; Wang et al., 2005; Liu et al., 2015; Li et al., 2021a), the Americas (Ersek et al., 2012; Bernal et al., 2016), and Africa (Thompson et al., 2002; Zielhofer et al., 2017b). This climate event is also visible in polar ice core records (Mayewski et al., 1997; Stuiver et al., 1997). Previous studies refer to it—or aspects of it—in various ways related to its chronology, including the 7.1 ka event (Aubán et al., 2016), 7.2 ka event (Zhang et al., 2021), 7.4 ka event (Fletcher et al., 2012), or ice-rafted debris (IRD)-5b event (Gronenborn, 2010). In this paper, we preliminarily refer to it as the "7.2 ka event" based on the peak timing of climate anomalies. Although the 7.2 ka event may be less pronounced than the other widely-acknowledged Holocene climate events, it is particularly interesting because it occurred during the Holocene Climate Maximum. It thus may provide useful analog for estimating the magnitude of climate changes under the increasing global warming of today.

Additionally, the 7.2 ka event represented by these paleoclimate records coincided with significant changes seen archaeologically in human societies throughout the world, such as the abandonment of a large number of sites, demographic shifts, and profound cultural transformations (Aubán et al., 2016). Specifically, the transition from the Mesolithic to the Neolithic across southern Iberia and the final collapse of the Early Neolithic Linear Pottery culture across central Europe were associated with climatic instability at around 7.4 ka BP (Gronenborn, 2010; Sánchez et al., 2012). In China, climatic deterioration between 7.6 and 7.0 ka BP coincided with considerable regional Neolithic cultural successions, particularly in the northerly latitudes, including those recognized across the Guanzhong Basin (Lü and Zhang, 2008), the Gansu-Qinghai region (Dong, 2013), the farming–grazing transitional zone (Zhang et al., 1997), and North China (Wang et al., 2014). The coincidence of archaeological evidence for such cultural changes with the 7.2 ka event suggests a possible link. Demonstrating climate change as a causative factor in these geographically widespread cultural changes, however, will require greater systematic knowledge about it.

For these reasons, it is necessary to have a detailed understanding of the 7.2 ka event. However, up to now, there has been no systematic review for this climate event. Here, we attempt to fill this gap through a synthesis of paleoclimate proxy records from various archives from the global. The use of widely-distributed paleoclimatic data avoids the risk of using data series from one area to extrapolate to others and thus provides a more complete and clearer climate picture (Shuman and Marsicek, 2016). In this paper, we synthesize well-dated and highly-resolved climate records from 58 globally-distributed sites. The aim of this synthesis is not only to compile high-quality data, but also to understand the temporal and spatial pattern of this climate event and to investigate the underlying climate-forcing mechanisms. Such a review can provide more robust climate background with which to explore human-environmental interactions during this climate anomaly period.

2. Site selection

Benefit of advances in paleoclimatic research, especially since the establishment of PAGES in 1991, a large number of paleoclimatic records have been published over the last three decades. In this work, we aim to understand the temporal and spatial pattern of the 7.2 ka event so we do not even attempt to list those studies that do not refer to it. The bias inherent in reporting occurrence and failing to report absence of the 7.2 ka event should be clear. We characterize records of interest as follows:

(1) the record covers the entire time interval of interest (7.6–7.0 ka BP);
(2) the record has a reliable chronological framework and high resolution (one control point every 2000 years; a record should have at least a sampling resolution of better than 100 years between 7.6 and 7.0 ka BP, and this cutoff is chosen so that the detection of a short term event would be feasible);
(3) the record includes proxies with a demonstrated relationship with climate variables based on knowledge of modern processes;
(4) the record is preferably multi-proxy (given that different proxies from the same record can yield different inferences about the timing, explanation, and magnitude of climatic change). In many, but far from all of these records, multi-proxy is included to provide accurate paleoclimate information for the 7.2 ka event.

With respect to the four criteria, 58 sites, including 18 lake sediments, one loess section, 16 speleothems, 18 marine sediments, and five ice cores, are selected for this review. For convenience of discussion, the 58 sites are grouped into five regions: Asia, the Americas, Europe and the Mediterranean, Africa, and the polar regions. In total 47 proxy time series from 42 sites are chose, but time series of the remaining 16 sites can't be obtained. Due to the complex relationship between climate variables and proxies, it is impossible to translate all proxies into quantitative or semi-quantitative climate signals. Therefore, in some cases, we follow the authors' original climate interpretations of the proxies and do not make any corrections. In addition, we also select 8 additional climate-forcing time series for exploring the underlying mechanisms. Numeric data for these time series are downloaded either from the National Oceanic and Atmospheric Administration (USA) (https://www.ncdc.noaa.gov/data-access/paleoclimatology-data), East Asian Paleoenvironmental Science Database (http://paleodata.ieecas.cn/index.aspx), or as digitized figures with GetData2.20 software (http://www.getdata-graph-digitizer.com/).

In this paper, we also use objective criteria for statistically detecting climate anomalies in 45 proxy time series from 40 sites (see Supplementary Material). The records of particle sizes for Wudongyang peat and soil $\delta^{18}O$ for Citelle Basin isn't carried out because of relatively coarse time resolution outside of the 7.6–7.0 ka BP and short time series, respectively. Since the focus of this study is on a centennial-scale climate event, the original proxy data are uniformly standardized by subtracting a 1000-yr moving average from the 200-yr moving average and normalizing the record using the standard deviation (SD) firstly (Wanner et al., 2011; Sagawa et al., 2014). If values of the processed proxy time series fall outside a 1 SD between 7.6 and 7.0 ka BP, we would conclude that evidence for the 7.2 ka event exists.

The details of the paleoclimate records discussed in this review are listed in Table 1, which includes the type of archive, dating material, number of dates, dating method, temporal resolution, and proxy type. Record locations are plotted on a map of the world to help visualize their spatial distribution (Fig. 1). Although the reviewed paleoclimate records have been dated by different method, the dates are corrected in original paper, providing a common chronological framework for intercomparison.

3. Proxy Records

In the following descriptions, we present relevant evidence from the various proxy records across the five regions.

3.1. Asia

The growing number of proxy records from the Asian summer monsoon domain, ranging from the beginning to the end of the

Table 1
Details for the proxy records reviewed in this study.

No.	Site	Longitude	Latitude	Archive	Dating material	Dating method	No. of dates	Time interval (ka BP)	Resolution (yr)	Proxy	Reference
1	Dongge	108.50	25.17	cave	speleothem	U-TH	45	9.0–0	5	$\delta^{18}O$	Wang et al., 2005
2	Shuiming	107.47	29.47	cave	speleothem	U-TH	10	8.0–7.0	2.7	$\delta^{13}C$, trace element	Feng et al., 2019
3	Qingtian	110.22	31.20	cave	speleothem	U-TH	31	10.9–6.1	2–6	$\delta^{18}O$	Liu et al., 2015
4	Magou	113.23	34.19	cave	speleothem	U-TH	66	11.7–1.1	4	$\delta^{18}O$	Cai et al., 2021
5	Tianmen	90.40	30.55	cave	speleothem	U-TH	10	8.7–4.3	3–7	$\delta^{18}O$	Cai et al., 2012
6	Baluk	84.44	42.26	cave	speleothem	U-TH	15	8.4–2.7	23	$\delta^{18}O$	Liu et al., 2019
7	Qinghai	100.08	36.32	lake	organic matter/ seed/plant macrofossils	AMS^{14}C	57	32.0–0	56	monsoon index	An et al., 2012
8	Dulan	98.20	36.10	loess section	loess	OSL	11	9.5–0	81	multi-proxy	Li et al., 2021b
9	Altai	88.21	48.70	lake	cellulose	AMS^{14}C	22	11.0–0	45	$\delta^{13}O$	Huang et al., 2020
10	Dadiwan	105.80	35.02	lake	organic matter	AMS^{14}C	12	16.0–1.0	12	Rb/Sr	Liu et al., 2020b
11	Bohai Sea	118.01	39.28	sea core	carbonized reed	AMS^{14}C	11	8.2–7.0	5	pollen	Zhao et al., 2021
12	Yangtze River	118.48	32.17	lake	plant remains	AMS^{14}C	11	9.0–7.2	5	phytolith	Zuo et al., 2021
13	Wangdongyang	119.38	27.40	lake	plant macrofossils peat	AMS^{14}C	9	8.3–1.0	45–85	multi-proxy	Zhao et al., 2022
14	Daihai	112.40	40.35	lake	organic matter	AMS^{14}C	9	12.0–0	23–158	pollen	Xu et al., 2003
15	B-Y14	122.55	39.24	sea core	organic matter foraminifer	AMS^{14}C	10	9.0–0	55	$U^{K'}_{37}$	Nan et al., 2017
16	A03-B	123.38	35.28	sea core	foraminifer	AMS^{14}C	7	8.8–0	29	TEX^{L}_{86}	Li et al., 2021a
17	KY07–04-01	128.56	31.38	sea core	foraminifer	AMS^{14}C	14	18.0–0	28–50	Mg/Ca	Kubota et al., 2010
18	A7	126.58	27.49	sea core	foraminifer	AMS^{14}C	16	18.0–0	48	$\delta^{13}O$	Xiang et al., 2007
19	OKI-151	125.52	26.11	sea core	foraminifer	AMS^{14}C	12	13.3–0	150	TEX^{H}_{86}, $U^{K'}_{37}$	Xu et al., 2018
20	Leizhou Peninsula	109.55	20.14	sea core	reef	TIMS	9	7.5–7.0	sub-annual	Sr/Ca	Yu et al., 2004
21	Ximenglongtan	99.35	22.38	lake	plant macrofossils	AMS^{14}C	12	9.4–0	10–20	multi-proxy	Ning et al., 2017
22	Xihu	100.04	26.01	lake	cellulose organic matter	AMS^{14}C	26	11.0–3.0	18	multi-proxy	Xu et al., 2015
23	Oman	59.48	21.55	sea core	foraminifer	AMS^{14}C	14	9.0–6.0	20	SST	Munz et al., 2017
24	Arabian Sea	57.36	18.03	sea core	foraminifer	AMS^{14}C	15	11.1–0	30	planktic foraminifer	Gupta et al., 2005
25	Hoti	57.21	23.05	cave	speleothem	U-TH	12	9.6–6.1	4	$\delta^{18}O$	Neff et al., 2001
26	Qunf	54.18	17.10	cave	speleothem	U-TH	18	10.3–0.4	4–5	$\delta^{18}O$	Fleitmann et al., 2003
27	Mawmluh	91.52	25.15	cave	speleothem	U-TH	12	12.5–3.6	5	$\delta^{18}O$	Berkelhammer et al., 2012
28	Nordan's Pond	−53.36	49.90	lake	plant macrofossils	AMS^{14}C	10	8.5–0	~100	composite proxy	Hughes et al., 2006
29	Pink Panther	−105.17	32.08	cave	speleothem	U-TH	22	12.3–0	17	$\delta^{18}O$	Asmerom et al., 2007
30	Oregon	−123.25	42.05	cave	speleothem	U-TH	29	13.0–0	3	$\delta^{18}O$	Ersek et al., 2012
31	Soledad Basin	−112.70	25.20	sea core	foraminifer	AMS^{14}C	22	13.9–0	50	Mg/Ca	Marchitto et al., 2010
32	Florida Straits	−83.13	24.24	sea core	foraminifer	AMS^{14}C	7	10.5–1.5	25	planktic foraminifera	Schmidt et al., 2012
33	Botuverá	−49.09	−27.13	cave	speleothem	U-TH	13	9.0–0	sub-annual	$\delta^{18}O$	Bernal et al., 2016
34	Lapa Grande	−44.21	−14.25	cave	speleothem	U-TH	24	10.2–1.3	10	$\delta^{18}O$	Stríkis et al., 2011
35	Titicaca	−69.26	−15.57	lake	organic matter	AMS^{14}C	9	13.0–1.0	45	$\delta^{13}C$	Baker et al., 2005
36	El Junco Lake	−91.00	−0.30	lake	organic matter	AMS^{14}C	21	9.0–0.0	5–50	botryococcenes	Zhang et al., 2014
37	North Atlantic	−14.43	55.28	sea core	foraminifer	AMS^{14}C	59	12.0–0	40	hematite-stained grains	Bond et al., 2001
38	Tsuolbmajavri	22.05	68.41	lake	plant macrofossils	AMS^{14}C	14	13.0–1.0	50–70	diatom	Korhola et al., 2000
39	Nordic Seas	−17.57	66.59	sea core	foraminifer	AMS^{14}C	10	10.2–0	80	alkenone	Bendle and Rosell-Mele, 2007
40	Suminko	17.47	54.11	lake	plant macrofossils	AMS^{14}C	13	13.0–0	90	pollen/ geochemistry	Pędziszewska et al., 2015
41	Citelle	5.12	45.41	lake	charcoal	AMS^{14}C	23	8.5–7.0	50	geochemistry	Berger et al., 2016
42	Accesa	10.53	42.59	lake	plant macrofossils/ tephra layer	AMS^{14}C	17	12.0–0	50	sedimentological analyses	Magny et al., 2007
43	Nova Grgosova	15.40	45.49	cave	speleothem	U-TH	28	10.0–0	21	$\delta^{18}O$, $\delta^{13}C$	Surić et al., 2021
44	Lago Preola	12.38	37.37	lake	peat	AMS^{14}C	8	11.0–0	64	sedimentological analyses	Magny et al., 2011
45	Padul	−3.36	37.00	lake	plant remains	AMS^{14}C	17	11.6–0	65	pollen	Ramos-Román et al., 2018

(*continued on next page*)

Table 1 (*continued*)

No.	Site	Longitude	Latitude	Archive	Dating material	Dating method	No. of dates	Time interval (ka BP)	Resolution (yr)	Proxy	Reference
46	Grotta di Carburangeli	13.16	38.17	cave	speleothem	U-TH	11	9.9–1.0	4	$\delta^{18}O$	Frisia et al., 2006
47	Jeita	35.39	33.57	cave	speleothem	U-TH	63	20.0–0	7	$\delta^{18}O$, $\delta^{13}C$, Sr/Ca	Cheng et al., 2015
48	Adriatic Sea	17.37	41.17	sea core	foraminifera	AMS^{14}C	10	11.5–0	40	$\delta^{18}O$	Siani et al., 2013
49	MD04-2797CQ	11.40	36.57	sea core	foraminifer	AMS^{14}C	13	18.0–2.0	less 100	pollen	Desprat et al., 2013
50	MD95–2043	−2.37	36.90	sea core	foraminifera	AMS^{14}C	9	11.7–1.3	100	pollen	Fletcher et al., 2012
51	MS27PT	29.27	31.47	sea core	foraminifera	AMS^{14}C	9	10.0–0.0	100	geochemistry/ grain-size	Revel et al., 2010
52	SL112	34.39	32.44	sea core	foraminifera	AMS^{14}C	4	12.0–4.0	100	Ba/Ca	Weldeab et al., 2014
53	Sidi Ali	−5.00	33.03	lake	plant macrofossils/ pollen	AMS^{14}C	26	12.0–0	80	geochemistry	Zielhofer et al., 2017a
54	Kilimanjaro	37.21	−3.04	ice core	ice	Model	–	11.7–0	50	dust flux	Thompson et al., 2002
55	GISP2	−38.50	72.60	ice core	ice	Layer counting	–	10.0–0	20, 0.5–2.5	$\delta^{18}O$, Na^+, K^+, Ca^{2+}	Mayewski et al., 1997 Stuiver et al., 1997
56	GRIP	−37.64	72.59	ice core	ice	Layer counting	–	11.7–0	20, 85	$\delta^{18}O$, CH_4	Vinther et al., 2006 Blunier et al., 1995
57	NGRIP	−42.32	75.10	ice core	ice	Layer counting	–	16.5–0	20	$\delta^{18}O$	Rasmussen et al., 2008
58	Taylor Dome	158.43	−77.47	ice core	ice	Model	–	11.0–0	10	$\delta^{18}O$	Steig et al., 2000

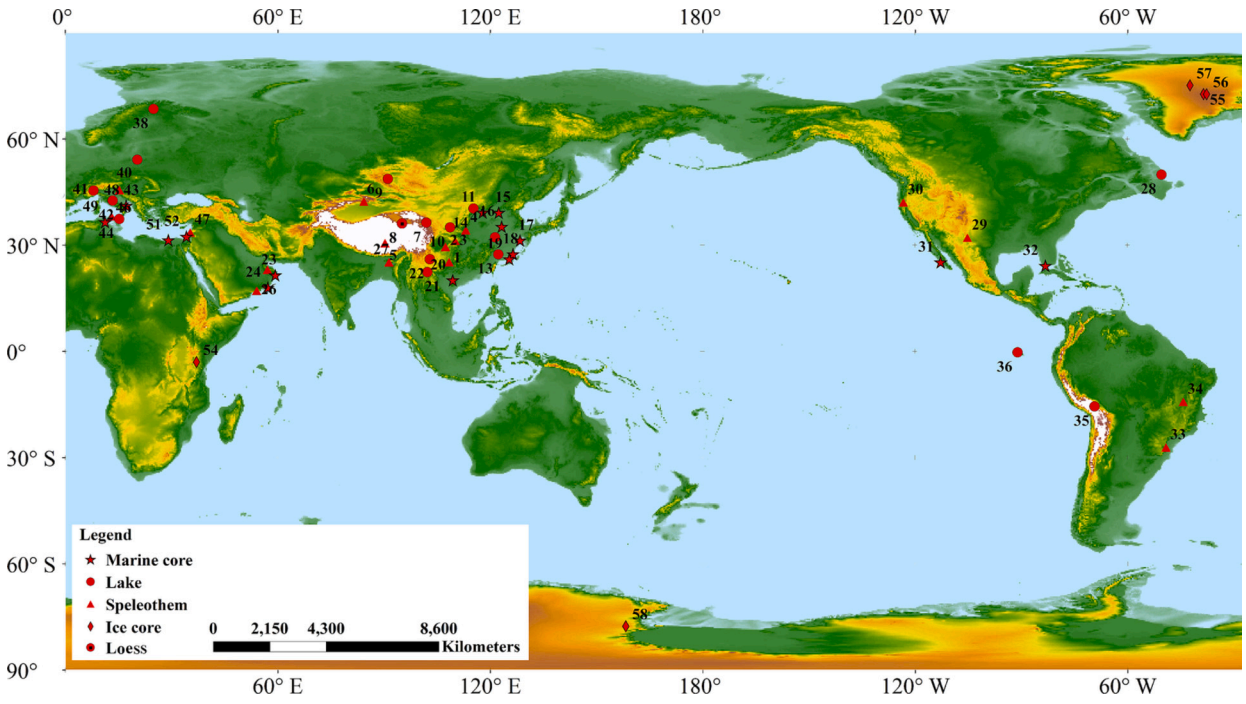

Fig. 1. Map of the site locations reviewed. The different shapes represent different types of paleoclimatic archives (stars: marine sediments; circles: lake sediments; triangles: speleothems; diamonds: ice cores; circle+dot: loess section).

Holocene, provide excellent information about past climate change. For the region of Asia, one area with a relatively high concentration of sites is associated with China, which boasts the highest density of speleothem studies. In southern China, a $\delta^{18}O$ record at 5-year sampling resolutions.

from an absolutely-dated speleothem from Dongge Cave shows a century-scale sharp monsoon anomaly centered at 7.2 ka BP (Wang et al., 2005; Fig. 2a). Similarly, a multi-proxy speleothem record of $\delta^{13}C$ and trace elements from Shuiming Cave, southwest China, also reveals a weak summer monsoon during the period of 7.3–7.1 ka BP (Feng et al., 2019). In central China, a speleothem record with a temporal resolution of 2 to 6 years from Qingtian Cave reveals a very fast onset event, evidenced by a marked anomaly in oxygen-isotopic composition between 7.4 and 7.2 ka BP (Liu et al., 2015; Fig. 2b). In northern China, a $\delta^{18}O$ record at a 4-year resolution from a precisely-dated speleothem from Magou Cave shows two century-scale sharp anomalies centered at 7.35 ka BP and 7.08 ka BP, respectively (Cai et al., 2021; Fig. 2c). Further west, on the Tibetan Plateau, a $\delta^{18}O$ record at a 3-to-7-year resolution from a precisely-dated speleothem from Tianmen Cave indicates a

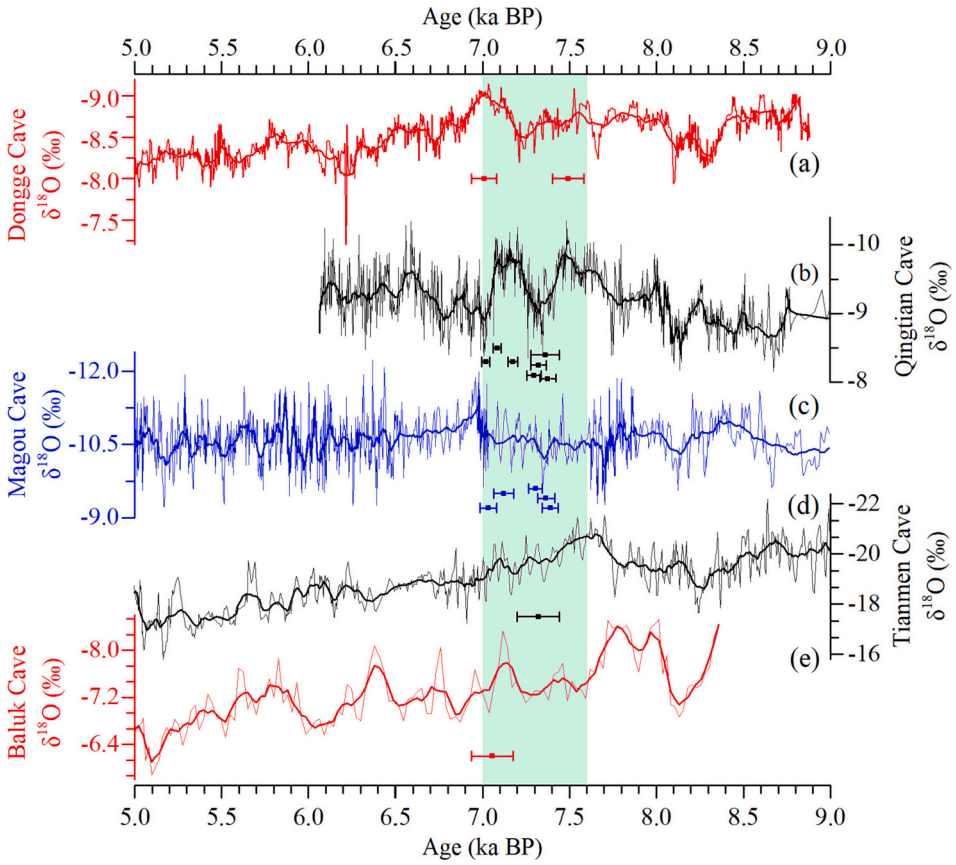

Fig. 2. Proxy time series for speleothem records from the East Asian summer monsoon domain. (a) Speleothem $\delta^{18}O$ for Dongge Cave, southern China (Wang et al., 2005); (b) Speleothem $\delta^{18}O$ for Qingtian Cave, central China (Liu et al., 2015); (c) Speleothem $\delta^{18}O$ for Magou Cave, central China (Cai et al., 2021); (d) Speleothem $\delta^{18}O$ for Tianmen Cave, southern Tibetan Plateau (Cai et al., 2012); (e) Speleothem $\delta^{18}O$ for Baluk Cave, northwestern China (Liu et al., 2019).

prominent oxygen-isotopic shift to positive values centered at 7.3 ka BP (Cai et al., 2012; Fig. 2d). The $\delta^{18}O$ value shift in these speleothem records reflects a weaker East Asian summer monsoon between 7.6 and 7.0 ka BP. In arid Central Asia, dominated by westerly circulation, a $\delta^{18}O$ record at a 23 year resolution from a precisely dated speleothem from Baluk Cave in Xinjiang Province also indicates abrupt hydroclimatic shifts during 7.6–7.1 ka BP (Liu et al., 2019; Fig. 2e).

Additional evidence for a weakened summer monsoon is also apparent in lacustrine records. At Qinghai Lake, the monsoon indices derived from the $CaCO_3$ content and total organic carbon reveals monsoon intensity decrease at 7.3 ka BP (An et al., 2012; Fig. 3a). Multiproxy inferred precipitation records from nearby Dulan loess section also show a period of low rainfall between 7.5 and 7.0 ka BP (Li et al., 2021b; Fig. 3b). Pronounced declines in the Rb/Sr ratio in the sediment from the Dadiwan section are assumed to reflect a weak summer monsoon interval around 7.3 ka BP (Liu et al., 2020b; Fig. 3d). A declining monsoon leads to a fundamental environmental shift. Base on pollen in two cores from Bohai Bay, Zhao et al. (2021) find the pronounced low percentage of broadleaved trees at 7.6–7.2 ka BP. Additionally, recent analyses of phytolith records in the Lower Yangtze indicate a short-lived intervals of bamboo decline at 7.3 ka BP (Zuo et al., 2021). Farther south, the magnitude of this environmental change is mirrored in the Wangdongyang Peat in southeast China, as evidenced by reductions in the forest cover and sediment particle sizes from 7.5 to 7.2 ka BP (Zhao et al., 2022; Fig. 3e).

Several quantitative reconstructions of temperature are made covering the interval of 7.6–7.0 ka BP in East Asia. Collectively these records show strong evidence for pronouncedly reduced temperature. At the present marginal zone of the East Asian summer monsoon, robust quantitative estimates of the Holocene climate using a pollen-based model indicate a sharp cooling of roughly 2 °C in inferred July temperature at 7.6 and 7.4 ka BP (Xu et al., 2003; Fig. 3f). Two records from the Yellow Sea include $U^{K'}_{37}$-inferred temperatures (Nan et al., 2017; Fig. 3g) and TEX^{L}_{86}-inferred temperatures (Li et al., 2021a; Fig. 3h), both of which reveal a cooling event at 7.2 ka BP and 7.6–7.3 ka BP, respectively. In the interior of China, negative excursions in peat α-cellulose $\delta^{13}O$ from the Altai Mountains are interpreted as resultant from relatively cold conditions at 7.15–7.05 ka BP (Huang et al., 2020; Fig. 3c).

The marine records from the Okinawa Trough are particularly interesting because they are influenced by the East Asian monsoon system, cold coastal waters, and sea-level changes. Several studies reconstruct sea surface temperature (SST) in the Okinawa Trough. In the northern Okinawa Trough, reconstructions of SST changes from Mg/Ca records (Kubota et al., 2010; Fig. 3i) suggest a cold event featuring reductions in the summer SST between 7.2 and 7.0 ka BP. Similarly, the $\delta^{18}O$ of planktonic foraminifers *G. ruber* from a marine sediment in the central Okinawa Trough suggests a cool event at 7.3 ka BP (Xiang et al., 2007). Another core in the central Okinawa Trough, a tetraether-inferred temperature reconstruction indicates a progressive cooling of 5 °C centered at 7.3 ka BP (Liu et al., 2020a). In the southern Okinawa Trough, the $U^{K'}_{37}$ and TEX^{H}_{86}-based temperature reconstruction suggests an overall decline of 3 °C and 3–14 °C, respectively (Xu et al., 2018; Fig. 3j). This cold event could be caused by an abrupt decrease in the strength of the Kuroshio Current, a signal that is recently discovered in sediment from the northern Okinawa Trough (Zheng et al., 2016).

Interestingly, the Kikai Akahoya (K-Ah) Ash dated at 7.3 ka BP (Smith et al., 2013) is detected in the majority of cores from the Okinawa Trough, indicating great potential of a volcanic eruption synchronizing these events.

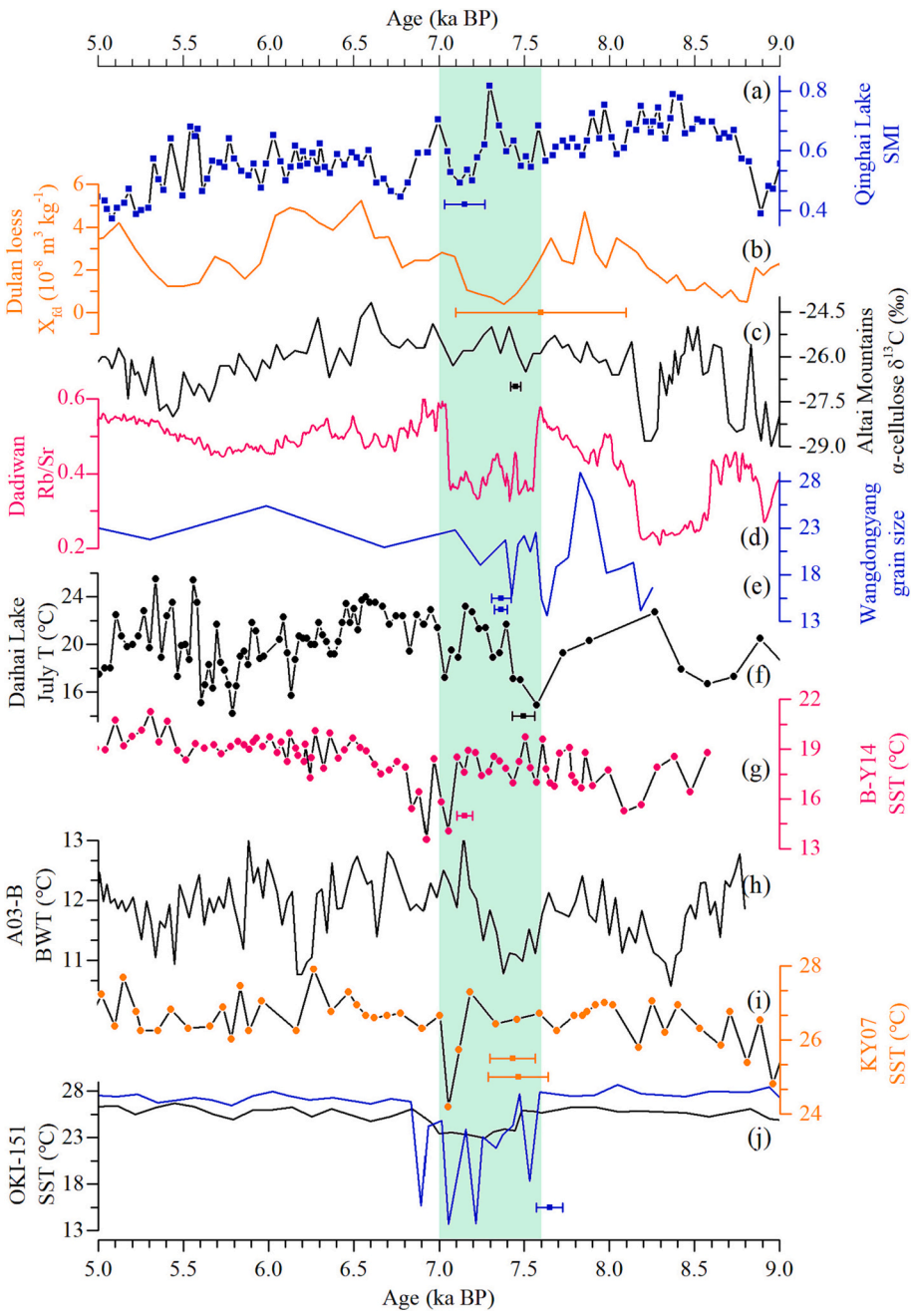

Fig. 3. Proxy time series for other records from the East Asian summer monsoon domain. (a) A composite summer monsoon index for Qinghai Lake, northeastern Tibetan Plateau (An et al., 2012); (b) Magnetic susceptibility for Dulan loess, northeastern Tibetan Plateau (Li et al., 2021b); (c) α cellulose $\delta^{13}C$ for a peat from Altai Mountains, northwest China (Huang et al., 2020); (d) Rb/Sr for Dadiwan, western Chinese Loess Plateau (Liu et al., 2020b); (e) Particle sizes for Wudongyang peat, southeast China (Zhao et al., 2022); (f) A July temperature reconstruction for Daihai Lake, northern China (Xu et al., 2003); (g) Sea surface temperature (SST) from $U^{K'}_{37}$ for core B—Y14, Yellow Sea (Nan et al., 2017); (h) Bottom water temperature (BWT) form TEX^{L}_{86} for core A03-B, Yellow Sea (Li et al., 2021a); (i) SST from Mg/Ca for core KY07–04-01, northern Okinawa Trough (Kubota et al., 2010); (j) SST from TEX^{H}_{86} (blue) and $U^{K'}_{37}$ (black) for core OKI-151, southern Okinawa Trough (Xu et al., 2018). (For interpretation of the references to colour in this figure legend, the reader is referred to the web version of this article.)

Farther south, a climate shift that characterizes the event is clearly identified on the Leizhou Peninsula in South China Sea, where an annually resolved Sr/Ca-based temperature reconstruction from a *Goniopora* reef profile suggests a winter temperature 2–3 °C colder than present between 7.5 and 7.0 ka BP (Yu et al., 2004). This result is strongly supported by microstructural examination of the *Goniopora* skeletons, which reveals at least nine massive, abrupt *Goniopora* mortality events resulting from winter cooling.

A broad Holocene monsoon minimum between 7.6 and 7.0 ka BP is also found in the Indian Summer Monsoon (ISM) domain. The well-dated, high-resolution geochemical and grain-size data from Lake Ximenglongtan, southwestern China, show a pronounced and prolonged drought interval between 7.6 and 7.0 ka BP (Ning et al., 2017). Another site in southwestern China records increases in bulk density, magnetic susceptibility, and carbonate fraction, indicating decreasing monsoon intensity at 7.5–7.1 ka BP (Xu et al., 2015). The most important records are perhaps those from offshore Oman. In the northern Oman margin, consistently low Mg/Ca-based and assemblage-based SST of *G. bulloides* suggest that ISM intensity is weaker at 7.6–7.4 ka BP (Munz et al., 2017; Fig. 4a). Another marine sediment core in the Oman records a distinct low percentage concentrations of fossil shells of the planktic foraminifer *G. bulloides* between 7.5 and 7.3 ka BP (Fig. 4b), indicative of a summer monsoon minimum (Gupta et al., 2005). These data parallel the short-term variations of the speleothem $\delta^{18}O$ record at near-by Hoti Cave (Fig. 4d), which indicates a decrease in rainfall at 7.5–7.2 ka BP (Neff et al., 2001), whereas a gradual increase in oxygen isotopes of a speleothem from Qunf Cave in southern Oman indicates the development of drier conditions after 7.5 ka BP under a weakening of the summer monsoon (Fleitmann et al., 2003; Fig. 4c). To the east, the highly resolved speleothem $\delta^{18}O$ data of Berkelhammer et al. (2012) from the Mawmluh Cave in northeastern India show a prominent shift to heavier values, indicating a monsoon reduction between 7.3 and 7.0 ka BP

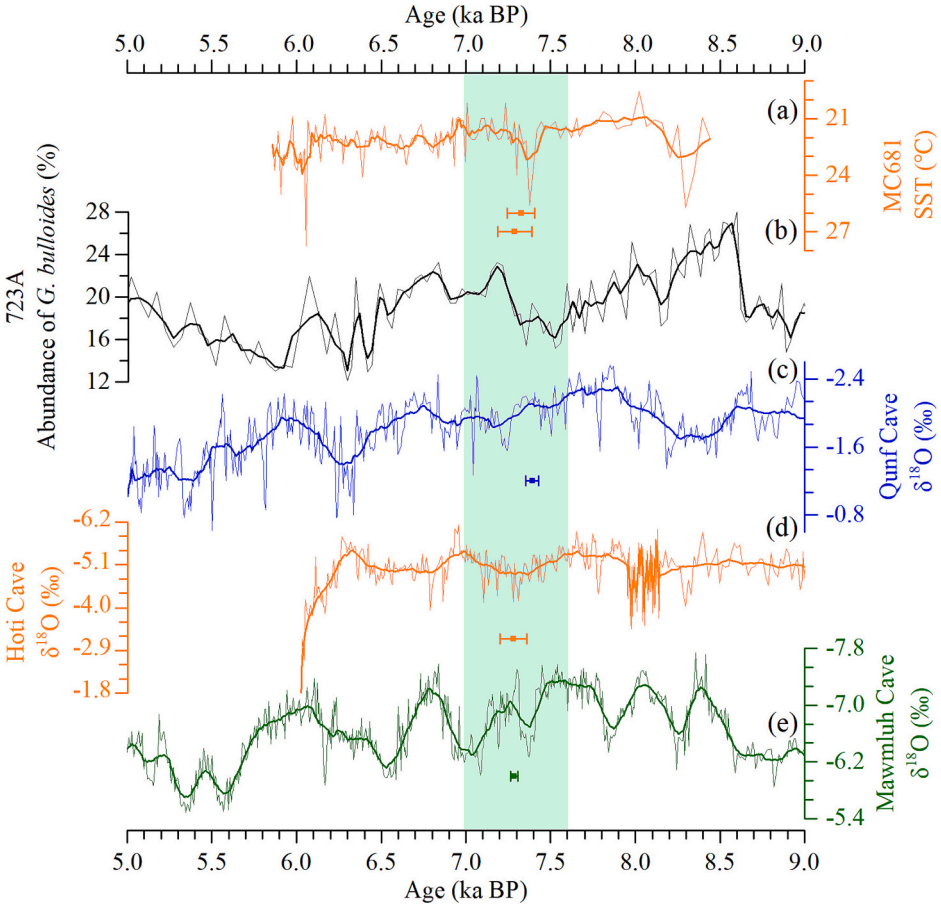

Fig. 4. Proxy time series for the South Asian summer monsoon domain. (a) Reconstructed SST from the Mg/Ca ratio of *G. bulloides* for core MC681, northern Oman (Munz et al., 2017); (b) Percentage of *Globigerina bulloides* for core 723A, northern Oman (Gupta et al., 2005); (c) Speleothem $\delta^{18}O$ for Qunf Cave, southern Oman (Fleitmann et al., 2003); (d) Speleothem $\delta^{18}O$ for Hoti Cave, northern Oman (Neff et al., 2001); (e) Speleothem $\delta^{18}O$ for Mawmluh Cave, northeastern India (Berkelhammer et al., 2012).

(Fig. 4e).

In summary, multiple paleoclimatic records across Asian show a climate event at 7.6–7.0 ka BP. It is marked by lowered temperature and weakened summer monsoon, which results in cold and dry conditions in much of this continent.

3.2. The Americas

In the northeast of North America, Hughes et al. (2006) analysis of plant macrofossils, testate amoebae, and peat humification in a peat profile from eastern Newfoundland, Canada, suggest colder and wetter conditions between 7.6 and 7.0 ka BP (Fig. 5a). Viau et al. (2006) complete an important reconstruction of July temperature from 752 fossil pollen records distributed across North America by using the modern analog technique, which reveals a cold interval centered at 7.5 ka BP. Mountain glaciers are sensitive indicators of environmental change and are likely to provide additional support for cooler temperatures. Menounos et al. (2009) summarize multi-proxy evidence of Holocene glacial fluctuations in the Canadian Cordillera and identify a glacial advance between 7.4 and 7.0 ka BP, which Ryder and Thomson (1986) refer to as the "Garibaldi Phase". Farther to the south, Asmerom et al. (2007) note prominent negative $\delta^{18}O$ excursions of a speleothem from the Pink Panther Cave in New Mexico, United States, possibly suggesting a strong increase in precipitation from 7.3 to 7.0 ka BP (Fig. 5b).

A study by Ersek et al. (2012) reconstructs Holocene climate variability using a high-resolution speleothem record from a cave in Oregon, United States. Significant anomalies in the oxygen and carbon isotopes at 7.4 ka BP (Fig. 5c) are interpreted as representative of dry conditions. Farther to the south, in the Soledad Basin, which is located off the west coast of Baja California Sur, Marchitto et al. (2010) provide a high-resolution Mg/Ca-based reconstruction of the SST to report five cold intervals between ~11 and 7 ka BP (Fig. 5d). One of these cold intervals occurs between 7.2 and 7.0 ka BP when increased oxygen isotope values appear in the Dongge Cave (Wang et al., 2005) and Hoti Cave (Neff et al., 2001), and increased IRD in the North Atlantic (Bond et al., 2001). In a high-time-resolution marine-sediment core from the Florida Straits, Schmidt et al. (2012) identify a period of increased sea surface salinity at 7.6 to 7.4 ka BP based on $\delta^{18}O$ of *Globigerinoides ruber* (Fig. 5e), which is associated with increased evaporation/precipitation ratios due to more arid conditions. The periods of climate anomalies developed are possibly related with the development of El Niño-like conditions in the eastern equatorial Pacific.

Paleoclimate records covering the interval of interest are relatively rare in the South American monsoon sector. Nevertheless, available speleothem and lake records suggest an intensification of monsoon precipitation from 7.6 to 7.0 ka BP. Bernal et al. (2016) present evidence, on the basis of the decreased Sr/Ca ratios of a speleothem from Botuverá Cave in southeastern Brazil, for increased precipitation centered at 7.2 ka BP (Fig. 5f). Similarly, Stríkis et al. (2011) find an anomaly in the oxygen-isotopic composition of a speleothem of about 1 per mil toward negative values in the Lapa Grande Cave in central-eastern Brazil, which is thought to be coincident with an increase in rainfall around 7.5–7.3 ka BP (Fig. 5g). Further west, Baker et al. (2005) use the carbon-isotopic composition of bulk organic matter to infer a high level of Lake Titicaca from 7.5 to 7.0 cal BP. Abrupt increases in South American monsoon are possibly associated with change in the behavior of El Niño-like conditions. A sediment core from El Junco Lake situated in the Galápagos Islands indicates a clear increase in El Niño activity between 7.6 and 7.4 ka BP (Zhang et al., 2014). Further south in southernmost South America, however, Pérez-Rodríguez et al. (2016) notes low Zr accumulation rates in sediment from Lago Hambre,

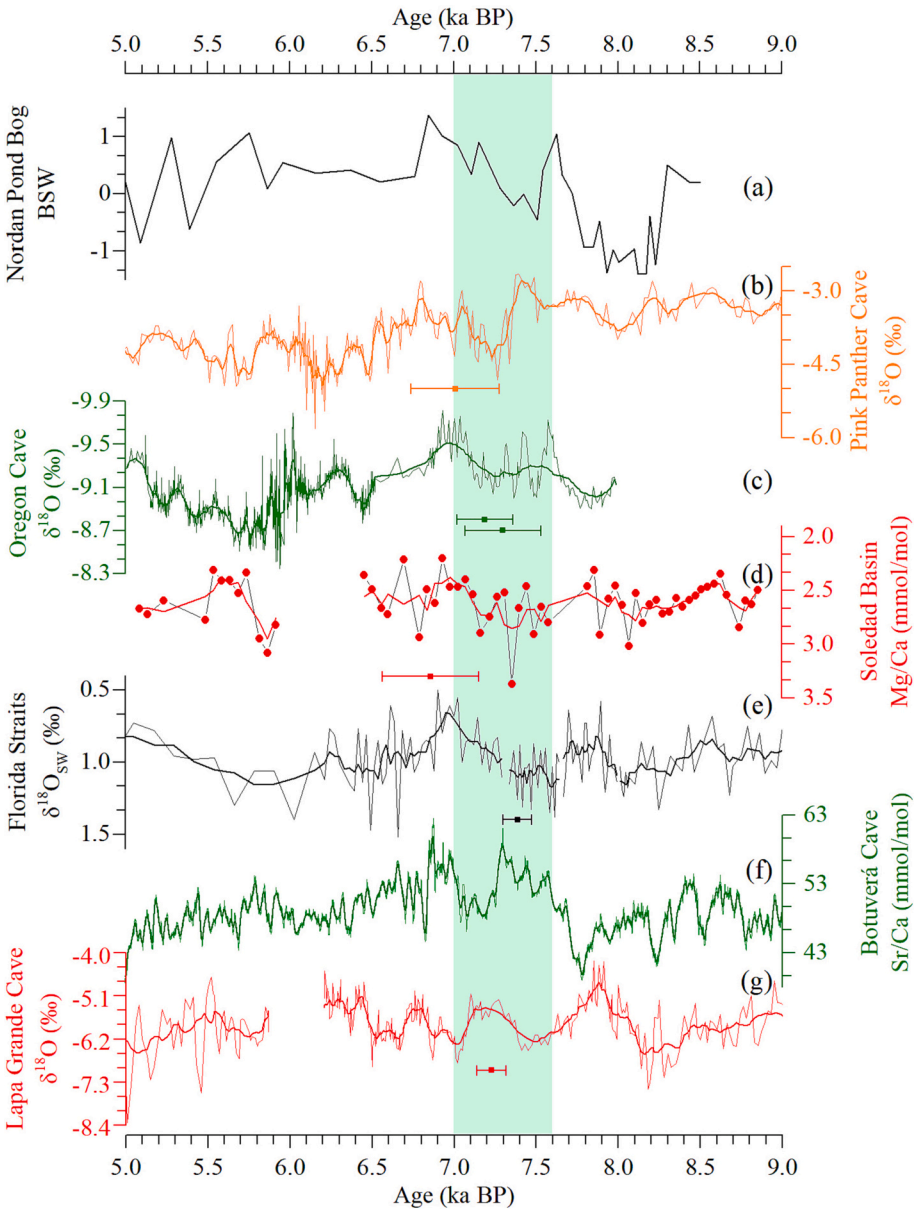

Fig. 5. Proxy time series for the Americas. (a) Composite bog surface wetness (BSW) for Nordan's Pond Bog, eastern Newfoundland (Hughes et al., 2006); (b) Speleothem $\delta^{18}O$ for Pink Panther Cave, southwestern United States (Asmerom et al., 2007); (c) Speleothem $\delta^{18}O$ for Oregon Cave, western United States (Ersek et al., 2012); (d) *G. bulloides* Mg/Ca for Soledad Basin (Marchitto et al., 2010); (e) Ice volume free *G. ruber* $\delta^{18}O_{SW}$ ($\delta^{18}O_{IVF\text{-}SW}$) for the Florida Straits (Schmidt et al., 2012); (f) Speleothem Sr/Ca for Botuverá Cave, southeastern Brazil (Bernal et al., 2016); (g) Speleothem $\delta^{18}O$ for Lapa Grande Cave, central-eastern Brazil (Stríkis et al., 2011). (For interpretation of the references to colour in this figure legend, the reader is referred to the web version of this article.)

indicating relatively dry conditions centered at 7.2 ka BP. In the same region, Menounos et al. (2013) combine AMS^{14}C dating of several leaves between two moraines with the age of Hudson tephra beyond the moraines to demonstrate a mountain glacial advance at that time.

Generally, climate anomalies associated with the 7.2 ka BP event show dry conditions across western, equatorial Pacific and Atlantic of North America but increased precipitation in northeastern and southwestern America. The South America monsoon region experiences wetter conditions.

3.3. Europe and the Mediterranean

For this region, a particularly revealing case is portrayed by a high-resolution IRD record from North Atlantic sediment cores. The record documents nine peaked events in the IRD during the Holocene, one of which occurs between around 7.6 and 7.3 ka BP (Bond et al., 2001; Fig. 6a), which Gronenborn (2010) terms the "IRD 5b-event." This result draws some support from a study of a sea core retrieved from the Faroe Islands that indicates a southward expansion of cold polar waters and drift ice into the North Atlantic at that time (Rasmussen and Thomsen, 2010), which facilitate the deposition of IRD. A diatom-based calibration model established for northern Fennoscandia suggests reduced summer temperatures at 7.2 ka BP (Korhola et al., 2000; Fig. 6b). This reconstruction is further supported by alkenone-inferred temperatures on the North Icelandic Shelf that indicate a sharp decrease of 2 °C between 7.1 and 6.9 ka BP (Bendle and Rosell-Mele, 2007). The same cooling event is displayed in sediment from Lake Sumink in northern Poland, where geochemical, diatom, and pollen data indicate a summer temperature decline between 7.6 and 7.5 ka BP (Pędziszewska et al., 2015). The occurrence of extended cold conditions may explain advances in mountain glaciers in Scandinavia centered roughly at 7.3 ka BP (Karlén, 1988; Nesje, 2009).

Farther to the south on the Swiss Plateau, pollen data from Lake Lago Basso indicate a timberline depression between 7.5 and 7.2 ka BP caused by temperature cooling (Haas et al., 1998). The reduced temperatures producing low evaporation favor for wetter conditions. At the northern edge of the Mediterranean, a multi-proxy study from the Rhone catchment area demonstrates the existence of a long tripartite rapid hydrological change at 7.7–7.1 ka BP (Berger et al., 2016; Fig. 6c). Farther east, a high-resolution lake-level reconstruction at Lake Accesa, north-

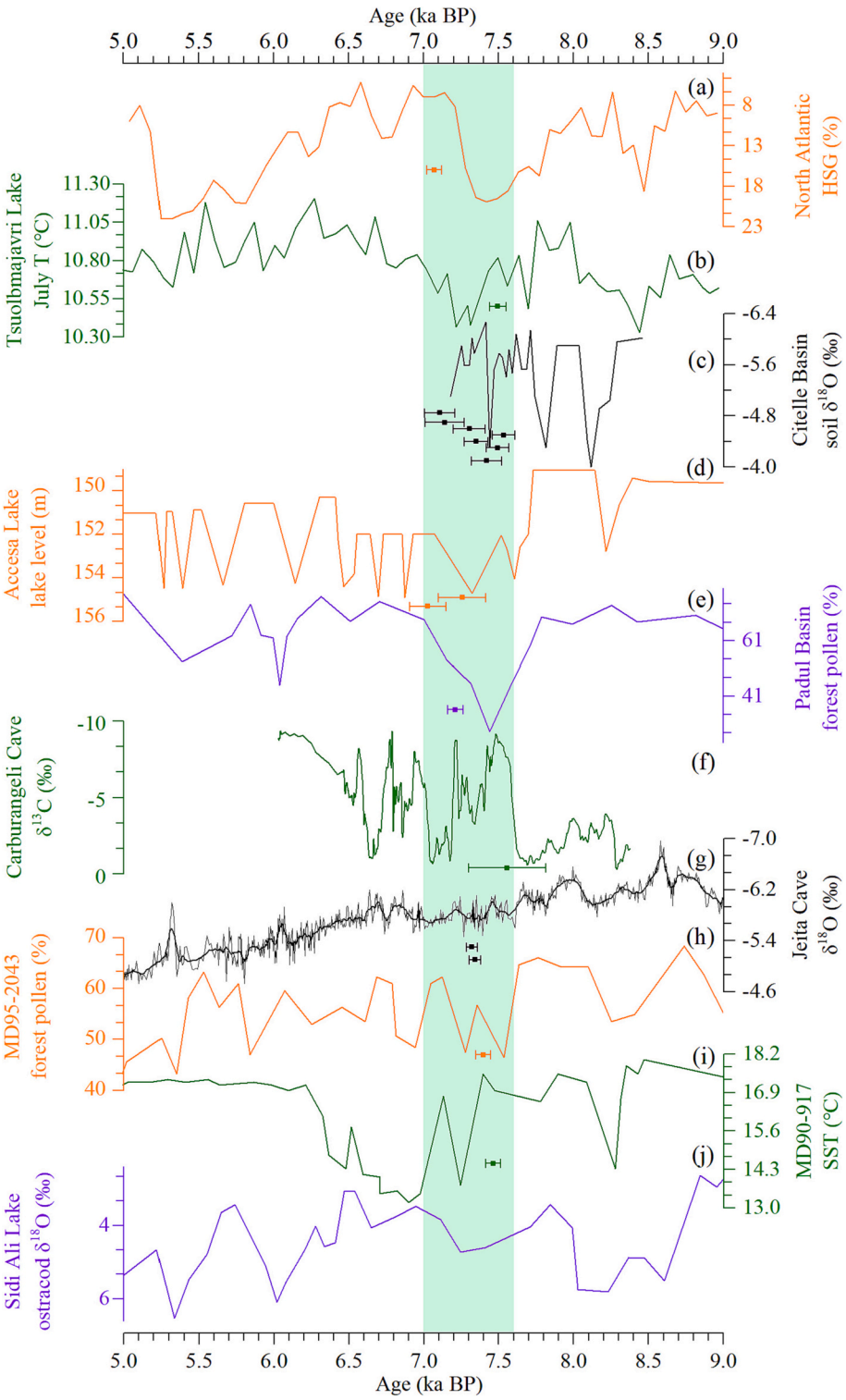

Fig. 6. Proxy time series for Europe, the Mediterranean, and Africa. (a) Hematite-stained grains (HSG) from the North Atlantic (Bond et al., 2001); (b) Reconstructed mean July temperatures from Lake Tsuolbmajavri, northern Fennoscandia (Korhola et al., 2000); (c) Soil $\delta^{18}O$ for Citelle Basin, southern France (Berger et al., 2016); (d) Lake-level reconstruction from Lake Accesa, northern Italy (Magny et al., 2007); (e) Mediterranean forest percentages from Padul Lake, southern Spain (Ramos-Román et al., 2018); (f) Speleothem $\delta^{13}C$ for Grotta di Carburangeli Cave, southern Italy (Frisia et al., 2006); (g) Speleothem $\delta^{18}O$ for Jeita Cave, Lebanon (Cheng et al., 2015); (h) Tree pollen for core MD95–2043, western Mediterranean (Fletcher et al., 2012); (i) SST from oxygen isotope of *G. bulloides* for core MD90–917, Adriatic Sea (Siani et al., 2013); (j) Ostracod $\delta^{18}O$ from Lake Sidi Ali, North African Middle Atlas (Zielhofer et al., 2017a).

central Italy, using a range of sedimentological analyses and level indicators shows a highstand around 7.3 ka BP (Magny et al., 2007; Fig. 6d). Other lakes in the region, such as Lake Ledro register a rising water level between 7.3 and 7.0 ka BP that coincides with a strong expansion of *Abies* pollen (Magny et al., 2012). This supports the earlier synthesis study of Magny (2004) who suggests a strong lake-level rise in central Europe between 7.5 and 7.0 ka BP. However, a prominent and abrupt increase of $\delta^{13}C$ values is observed in a speleothem from Nova Grgosova Cave, consistent with a decrease in precipitation at about 7.4 ka BP (Surić et al., 2021).

In contrast to these data, there is clear proxy evidence of decreased moisture in the south Mediterranean from 7.6 to 7.0 ka BP. In the southern Iberian Peninsula, a decrease in percentages of evergreen tree pollen around 7.6–7.3 ka BP is recorded in sediment from Padul Lake, suggesting a cold and dry climate (Ramos-Román et al., 2018; Fig. 6e). Farther east, the sedimentological analyses from which lake levels can be inferred to register a sharp fall in water level between 7.5 and 7.3 ka BP at Lago Preola in southern Sicily, Italy (Magny et al., 2011).

Approximately 75 km northeast of Lago Preola, a Holocene climate reconstruction is made from Grotta di Carburangeli, where high speleothem $\delta^{18}O$ excursions point to cold and dry climate conditions at approximately 7.5 ka BP (Frisia et al., 2006; Fig. 6f). This environmental signal is similarly recorded in the eastern Mediterranean where speleothem $\delta^{13}C$ and $\delta^{18}O$ data with a 7-year resolution from Jeita Cave in Lebanon show a prominent shift to higher values between 7.6 and 7.1 ka BP (Cheng et al., 2015; Fig. 6g). Taken with the records discussed above, the proxy evidence reveals a contrasting paleohydrological pattern between 7.6 and 7.0 ka BP in the Mediterranean. This pattern indicating inverse precipitation variability across the Mediterranean is also noted by Magny et al. (2013), who combine lacustrine and marine records from the central Mediterranean along a north–south transect.

Several studies also reveal possible imprints of the 7.2 ka event in sea cores from the Mediterranean. A dry interval in core MD95–2043 correlative with this event is indicated by the decreased forest pollen percentages between 7.6 and 7.4 ka BP (Fletcher et al., 2012; Fig. 6h). A marine pollen record from a core from the southern Central Mediterranean indicates noticeable changes in the herbaceous composition, as shown by an increase in Asteraceae at the expense of Cyperaceae between 7.3 and 7.0 ka BP (Desprat et al., 2013). A record of SST changes derived from the South Adriatic Sea indicates significant cooling between 7.5 and 7.3 ka BP, according to an assumed calibration of planktonic foraminifera and an isotopic paleothermometer (Siani et al., 2013; Fig. 6i). This dry and cold event is associated with the reactivation of the convective overturn and marked the end of sapropel S1 (Filippidi et al., 2016; Tesi et al., 2017).

Overall, there is clear evidence for a climate signal of the 7.2 ka BP event in north-central Europe, marked in general by cooling and increase in precipitation. A contrasting paleohydrological pattern occurs in the Mediterranean characterized by northern wetting and southern drying conditions.

3.4. Africa

Several studies have described palaeohydrological fluctuations of

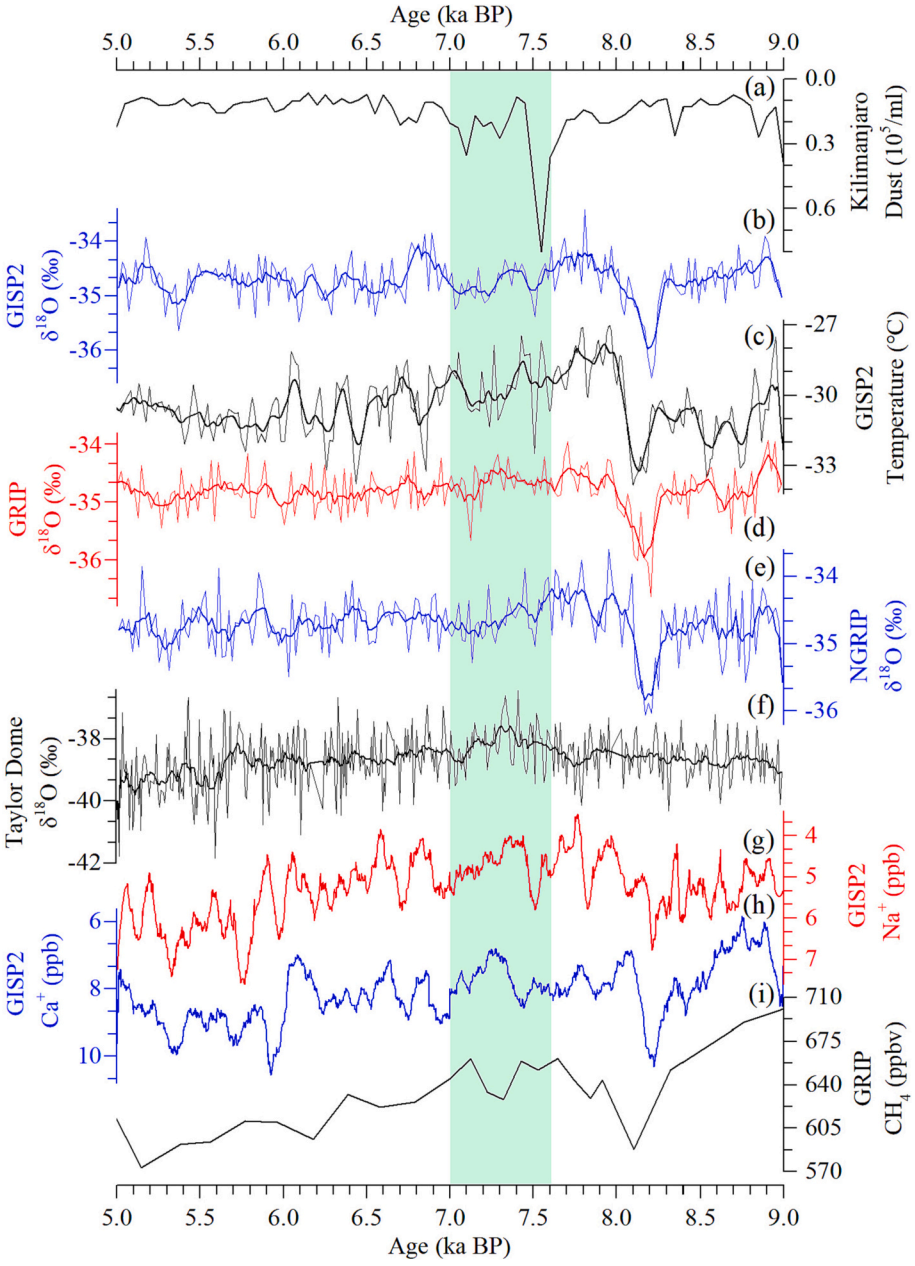

Fig. 7. Proxy time series for ice cores. (a) Dust flux for Mt. Kilimanjaro ice core (Thompson et al., 2002); (b) $\delta^{18}O$ for GISP2 (Stuiver et al., 1997). (c) Reconstructed temperature from argon and nitrogen isotopes for GISP2 (Kobashi et al., 2017); (d) $\delta^{18}O$ for GRIP (Vinther et al., 2006); (e) $\delta^{18}O$ for NGRIP (Rasmussen et al., 2008); (f) $\delta^{18}O$ for Taylor Dome (Steig et al., 2000); (g) Smoothed (100 yr) Na^{+} for GISP2 (Mayewski et al., 1997); (h) Smoothed (100 yr) Ca^{+} for GISP2 (Mayewski et al., 1997); (i) CH_4 for GRIP (Blunier et al., 1995).

North East Africa in the past. A high-resolution, multi-proxy analysis of sediments from the Nile margin indicates a decrease in Nile River contribution and an increase in aeolian Saharan contribution at approximately 7.5 ka BP (Revel et al., 2010). Planktonic foraminiferal Ba/Ca time series from the eastern Mediterranean Sea similarly reveals a remarkably gradual transition to a relatively low Nile River runoff after 7.5 ka BP (Weldeab et al., 2014). The Nile River discharge is fed by river flow from the Ethiopian Plateau, whose reduction is a direct marker of reduced rainfall in the Highlands, which is associated with the restricted southward migration of the Intertropical Convergence Zone. To the west, in the North African Middle Atlas range, proxy studies of lithogenic grain sizes and geochemistry on a 26 AMS^{14}C dates-constrained core from Lake Sidi Ali, indicate an enhanced Saharan dust supply into the lake at 7.3 ka BP (Zielhofer et al., 2017b). These proxies display similarities with the stable isotopes of ostracod shells in the same lake, indicating decreases in western Mediterranean winter rain (Zielhofer et al., 2017a; Fig. 6j). The isotopic and geochemical analyses of core ODP 658C retrieved on the continental slope off Northwest Africa also suggest that large amounts of aeolian dust are deflated from the Sahara to the eastern Atlantic between 7.5 and 7.0 ka BP (Cole et al., 2009). These data are paralleled by a high-altitude ice core record from Mt. Kilimanjaro, which reveals a peak in the aeolian dust precisely dated to 7.6–7.5 ka BP that is clearly deposited during an extremely arid period (Thompson et al., 2002; Fig. 7a).

Overall, the available proxy evidence in Africa suggests that an arid episode from 7.6 to 7.0 ka BP occurs midway through a prolonged humid period that begin in the early Holocene.

3.5. Polar regions

High-time-resolution and high-quality ice core records from the polar regions provide compelling evidence for 7.2 ka BP climate event. The most important climate signal is the occurrence of extreme values in the δ^{18}O of Greenland Ice Sheet Project 2 (GISP2) ice core, indicative of an air temperature trough during the period of 7.6–7.0 ka BP (Stuiver et al., 1997; Fig. 7b). Similarly, δ^{18}O from Greenland Ice Core Project (GRIP) and North Greenland Ice Core Project (NGRIP) ice cores also indicate of an air temperature trough (Vinther et al., 2006; Rasmussen et al., 2008; Fig. 7d and e). Recently, argon and nitrogen isotopes of trapped air in the GISP2 ice core are used to reconstruct Holocene temperatures and indicate colder climate conditions during this time period (Kobashi et al., 2017; Fig. 7c). Evidence also exists for colder temperatures in Antarctica, as evidenced by δ^{18}O values in the Taylor Dome (Steig et al., 2000; Fig. 7f).

Furthermore, signs of climate anomalies reflecting environmental conditions in other regions are often indicated in the polar ice core records. For example, sharp anomalies in major ion concentrations from the GISP2 ice core demonstrate a considerable change in atmospheric circulation during the period of 7.6–7.0 ka BP. Among these anomalies are increased levels of Na^+ and Ca^{2+} (Fig. 7g and h). These ions are caused by an expansion of the northern polar vortex, strengthening of the Siberian high, and intensification of the northern westerlies, which results in increased atmospheric loading of aerosols from dust sources over the ice sheet (Mayewski et al., 1997). A proxy for the wetland extent, namely the CH_4 concentration record derived from GRIP ice core, visually shows a reduction indicative of increased aridity of the tropical area between 7.4 and 7.3 ka BP (Blunier et al., 1995; Fig. 7i).

These ice core records collectively show that climate conditions change near synchronously in the polar regions and far from them, demonstrating that a widespread event occurs.

3.6. Summary

The 7.2 ka event is recorded in the different types of paleoclimate proxies from Asia, the Americas, Europe and the Mediterranean, Africa, and the polar regions. In the Asian monsoon domain, speleothem δ^{18}O and lacustrine proxy records show a summer monsoon reduction that is synchronous with a decline in temperature (Neff et al., 2001; Xu et al., 2003; Yu et al., 2004; Wang et al., 2005; An et al., 2012; Cai et al., 2012). Recently, a review of high-resolution hydrological records identifies an abrupt weakening of the East Asian and Australian summer monsoons around 7.2 ka BP (Zhang et al., 2021). Conversely, in the South American monsoon region, speleothem δ^{18}O records suggest an intensification of monsoon precipitation (Stríkis et al., 2011; Bernal et al., 2016). In west-south North America, dry climate conditions are evident in speleothem and sea cores records (Ersek et al., 2012; Schmidt et al., 2012). Changes in the amount of rainfall seen in proxy records from the several monsoon domains are manifested by a southward migration of the Intertropical Convergence Zone. In north-central Europe, an IRD spike (Bond et al., 2001), widespread mountain glacial advances (Karlén, 1988) and higher lake levels (Magny, 2004) point to cold–wet climate conditions. A pattern of opposing hydrological variability is apparently across the Mediterranean. In Africa, proxy records show clear indications of a dry interval, as evidenced by increased aeolian flux into the Atlantic coast of the Western Sahara and Kilimanjaro ice core (Thompson et al., 2002; Revel et al., 2010; Zielhofer et al., 2017a). In the polar regions, ice core records reveal intensified atmospheric circulation and generally lower temperatures (Mayewski et al., 1997; Stuiver et al., 1997; Steig et al., 2000).

We should stress that the strength of the climate signals tied to the 7.2 ka event vary from being relatively complacent to dramatic. The signals include such phenomena as a summertime cooling of 2 °C that led to a fundamental vegetation shift within the Daihai Lake catchment (Xu et al., 2003), and the overcooling of SSTs to below 18 °C that results in at least nine abrupt massive mortality events in reef corals (Yu et al., 2004). Our comparison among these records also indicates inconsistencies among the dating and timing of these signals related to the 7.2 ka event, but one should be cautious in ascribing too much significance to these age differences. We must bear in mind that detecting a close correspondence in timing for possible anomalous events can be difficult because such events often last only a few centuries and are evidenced across many and variable proxy records from widely separate places. This difficulty is also due in part to the different sample resolutions of the types of paleoclimate proxy records, which may range from several decades to several centuries. Each individual proxy record also contains dating error due to the methods of chronological determination and types of dating samples involved. In addition, the differences in the sensitivity of the climate proxies from record to record also explain why the signs, intensities, and timing of the 7.2 ka event can vary across different areas. As these inconsistencies are to be expected across multiple proxy records, we can thus still assert that the globally distributed signatures for climate change between 7.6 and 7.0 ka BP are sufficient to demonstrate an event with climate changes worldwide during this time period.

We also need to consider why the 7.2 ka event receives relatively little attention compared with other Holocene climate events. First, the 7.2 ka event occurs close in time to an 8.2 ka BP event. Fluctuations in proxy records occurring around 7.6–7.0 ka BP may be due to the effects of the terminating 8.2 ka BP event because of the relatively imprecise dating of early Holocene proxy data. Second, the magnitude of environmental and climatic change around 7.6–7.0 ka BP is too slight to be easily observed in the geological record, because the 7.2 ka event occurs during the Holocene Climate Maximum. The relatively high precipitation and temperature of this period could offset the cooling and drying impact of the 7.2 ka event. Third, not all the oscillations that apparently take place are visible in each of the available records: in many instances, this could be due to the fact that many records lack a sufficiently high time resolution and precise dating.

4. Possible causes for the 7.2 ka event

In order to get insight into the dynamics of the formation of the 7.2

ka event, the time series of the four most important climate forcing factors are represented in Fig. 8. In addition, the 7.2 ka event indicated in Fig. 2–7 is marked by cyan bar in Fig. 8.

4.1. Summer insolation

Although the 7.2 ka event on the multi-century timescale, it has been shown that the Holocene climate change is dominated by the influence of long-term trend change in summer insolation at the millennial timescale, which could impact on the occurrence of short-term climate events (Berger and Loutre, 1991; Wang et al., 2005). A prominent example of this control occurs during the early to mid-Holocene when higher-than-present Northern Hemisphere summer insolation render the North African monsoon strong enough to turn the Sahara Desert into a green and verdant landscape (deMenocal et al., 2000). High-resolution and absolute-dated speleothem $\delta^{18}O$ records from the Asian monsoon domain and the South American monsoon domain also indicate that long-term histories of summer monsoon intensity are associated with summer insolation (Fleitmann et al., 2003; Wang et al., 2005; Bernal et al., 2016). As indicated in Fig. 8h, the period of 7.6–7.0 ka BP evidences the gradual but the fastest decreasing rate of the annual Northern Hemisphere summer insolation (Berger and Loutre, 1991). Although progressive insolation changes alone are not likely to render such an abrupt climate change at 7.6–7.0 ka BP, paleoclimate modeling shows that subtle changes in insolation, aided by positive feedback from the atmosphere, ocean, sea ice, and vegetation, could produce significant climate shifts owing to the nonlinear reaction of the climate system (deMenocal et al., 2000). Studies indicate that the fastest rate of annual insolation decline during the 7.2 ka event also could promote a more unstable climate through rapidly changing thermal gradients at different latitudes (e.g. Zhao et al., 2010; Fig. 8g).

4.2. Solar activity

The second possible forcing factor is solar activity. The period of 7.6–7.0 ka BP is characterized by a series of negative total solar irradiance anomalies, generally larger than any others in the Holocene, as shown by the sharply high production of ^{14}C and ^{10}Be (Stuiver et al., 1998; Steinhilber et al., 2009; Fig. 8e). The causal path linking solar activity to the climate change follows several ways. Firstly, the most obvious mechanism for solar activity on the climate involves the direct effect of the observed variation in total solar irradiance on heating the Earth system (Gray et al., 2010). Model studies (Haigh, 1996) imply that at times of reduced solar irradiance, the relatively large reduction in incoming ultraviolet radiation causes decreases in lower stratospheric ozone formation, thus cooling this layer differentially with respect to latitude. These changes in stratospheric ozone induce a dramatic reorganization of tropospheric circulation patterns (Haigh, 1996). Secondly, the solar minimum also involves less heating of cloud-free areas of the subtropics, evaporating less moisture (Meehl et al., 2009). Thus, less moisture is carried by the trade winds to the convergence zones, where it would fuel intensification of the Hadley and Walker circulations. The two mechanisms act together to result in a southward migration of the Intertropical Convergence Zone and an increasingly El Niño-like state, generating widespread climate variability on centennial to millennial timescales (Haigh, 1996). During 7.6–7.0 ka BP, the close

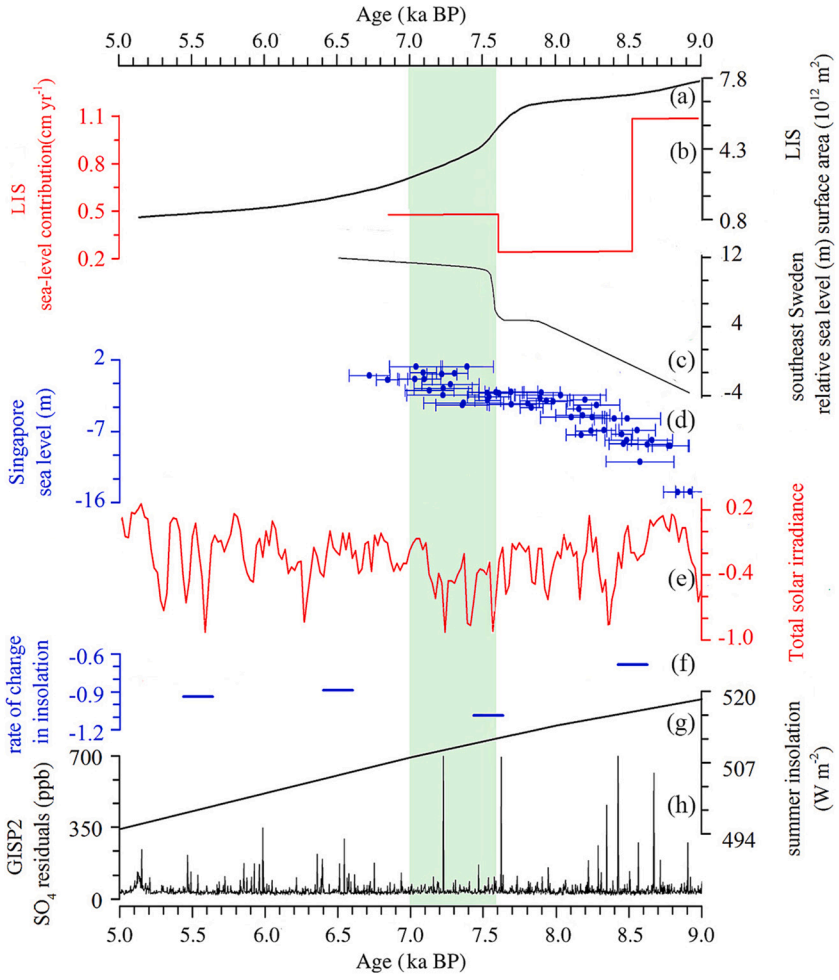

Fig. 8. Time series for climate-forcing. (a) The Laurentide Ice Sheet area (Dyke et al., 2003). (b) The Laurentide Ice Sheet sea-level contribution (Carlson et al., 2008). (c) Sea-level reconstruction for southeast Sweden (Yu et al., 2007). (d) Sea-level reconstruction for Singapore (Bird et al., 2007). (e) Total solar irradiance based on ^{10}Be, ^{14}C in tree rings and polar ice cores (Steinhilber et al., 2009). (f) The rate of change in annual insolation (Zhao et al., 2010). (g) Summer insolation at 60°N (Berger and Loutre, 1991). (h) SO_4 residuals for the GISP2 (Zielinski et al., 1996).

correspondence in timing of solar irradiance minima, positive speleothem $\delta^{18}O$ values in the Asian monsoon domain (Neff et al., 2001; Gupta et al., 2005; Wang et al., 2005; Cai et al., 2012), and negative speleothem $\delta^{18}O$ values in the South America monsoon region (Stríkis et al., 2011) supports the proposed relationship between solar forcing and climate change. Note that a southward migration of the Intertropical Convergence Zone cannot account for wet conditions in the North American monsoon region during 7.6–7.0 ka BP that are indicated by the speleothem $\delta^{18}O$ records from the southwestern United States (Asmerom et al., 2007). Asmerom et al. (2007) suggest that solar variability affects rainfall in the Asian monsoon region and the southwest in opposite ways through changes in climate systems of the tropical Pacific Ocean.

Additionally, the relationship between nuclide production rates (^{14}C and ^{10}Be) and drift ice deposition recorded in North Atlantic sediments leads to the suggestion that a significant part of the centennial- to millennial-scale climate variability during the Holocene is driven by solar forcing (Bond et al., 2001; Renssen et al., 2006). In fact, Goosse et al. (2002) suggest that variations in solar irradiance may trigger a reduction in North Atlantic Deep Water production resulting in climate anomalies quite similar in magnitude, duration, and spatial pattern to those due to freshwater forcing (Haug et al., 2001; Zhang and Delworth, 2005; Stríkis et al., 2011; Liu et al., 2013). Evidence that the interval of increased IRD in the North Atlantic (Bond et al., 2001) coincide with these episodes of increased sea surface salinity in the Florida Straits (Schmidt et al., 2012), strong lake-level rises in central Europe (Magny, 2004), positive speleothem $\delta^{18}O$ values in the Asian monsoon domain (Neff et al., 2001; Gupta et al., 2005; Wang et al., 2005; Cai et al., 2012), negative speleothem $\delta^{18}O$ values in the South American monsoon region (Stríkis et al., 2011), and decreased winter precipitation in northwest Africa (Zielhofer et al., 2017a) supports a strong coupling between North Atlantic cooling and the global climate.

4.3. Volcanic eruption

Another possible external forcing responsible for sharp anomalies between 7.6 and 7.0 ka BP is volcanic eruption. Large volcanic eruptions are well known to inject sulfur dioxide into the lower stratosphere, which forms sulfate-containing aerosol particles that affect both shortwave and longwave radiation (Zielinski et al., 1996; Robock, 2000). The disturbance to the radiation produces cooling at the surface but heating in the stratosphere (Robock, 2000). The dynamic response to the stratospheric heating would perturb the atmospheric circulation (Fischer et al., 2007; Ridley et al., 2015). Observations of significant continental-scale summer cooling over Europe occurring during the year of historically-recorded volcanic eruptions and persisting for 1–2 more years support this hypothesis (Fischer et al., 2007). In addition to temperature changes, studies suggest that after large volcanic eruptions in the tropics, precipitation apparently changes because of a positive phase of the North Atlantic Oscillation (NAO) (Fischer et al., 2007) and the southward migration of the Intertropical Convergence Zone (Ridley et al., 2015). While the lasting influence on the regional climate clearly outlives the short residence time of stratospheric sulfate aerosols from a single eruption, recent climate model simulations indicate this effect lasts longer, with a single large volcanic eruption able to induce rapid atmospheric and ocean surface cooling that persist approximately 16 years (Kobashi et al., 2017). Furthermore, a series of large volcanic eruptions even could induce decadal to centennial low temperatures at high northern latitudes owing to sea ice and ocean feedback (Miller et al., 2012; Sigl et al., 2015).

Coincident with the timing of the climate shift of the 7.2 ka event was the large eruption of Mount Mazama, which deposited ash in GISP2 ice core precisely dated to 7627 ± 150 BP. Zdanowicz et al. (1999) suggested that this eruption led to a total stratospheric aerosol loading of between 88 and 224 Mt. and produced a temperature depression of ~0.6 to 0.7 °C at mid to high northern latitudes for 1–3 years. These results indicate that the eruption is one of the most climatically significant volcanic events of the Holocene in the Northern Hemisphere, and it may have led to substantial stratospheric ozone depletion. The other significant volcanic eruption, known as the K-Ah (VEI = 7.2), has been precisely constrained to 7303–7165 BP (Smith et al., 2013). It produced one of the most widespread Holocene tephras in East Asia, dispersing a bulk volume of 170 km^3 ash over an extensive lobe with an axis length of 1300 km, mantling an area from southern to central Japan and the adjacent seas (Machida, 1999). As suggested by Fig. 8i, the high number of volcanic eruptions likely occurred between 7.6 and 7.0 ka BP. This could have triggered to the widespread cooling, weaker Asian summer monsoon, stronger South American summer monsoon, and wetter conditions in north-central Europe, as observed in proxy records (Man et al., 2014; Zhao et al., 2015; Xu et al., 2018).

4.4. Laurentide Ice Sheet retreat

Lastly, the retreat of the Laurentide Ice Sheet (LIS) could also act as a possible causal factor. Carlson et al. (2008) use a rich data set of radiocarbon dates and ^{10}Be ages to infer a retreat of the Laurentide Ice Sheet between 7.6 and 7.0 ka BP. This is supported by geologic evidence from the Labrador Sea that suggest an accelerated Laurentide Ice Sheet retreat between 7.6 and 7.0 ka BP (Dyke et al., 2003; Fig. 8a). Likewise, Ullman et al. (2016) find that the dominant loss of the Laurentide Ice Sheet volume leads to the separation of the Labrador Dome into two domes by 7.6 ka BP. This recession leads to the formation of numerous glacial lakes, which drain in approximately 16 meltwater pulses with fluxes exceeding 0.015 Sv into the ocean (Jansson and Kleman, 2004).

The global sea-level rise at that time demonstrates frequent meltwater discharge and sudden increase in ocean mass. For example, a rapid sea-level rise of ~4.5 m is found at 7.6 ka BP by dating the transgression and regression in marginal basins of the southeastern Swedish Baltic Sea (Yu et al., 2007; Fig. 8c). Carlson et al. (2008) estimate sea level rise at an average rate of about 0.7 cm yr^{-1} between 7.6 and 7.0 ka BP (Fig. 8b). The Black Sea is reconnected with the global ocean between 7.5 and 7.0 ka BP, providing indirect proof of the rapid sea-level rises (Herrle et al., 2018). Recent work from the Po Delta indicates a sharply transgressive phase starting at 7.7 ka BP (Amorosi et al., 2017; Bruno et al., 2017). This rapid sea-level rise is also identified in regions remote from the ice-loading effects. A pollen record from the northwest coast of Bohai Bay, northern China, suggests that a large number of halophytes, mainly Chenopodiaceae, sharply increase at 7560–7460 BP (Zhao et al., 2021), mirroring sea level rise (Xu et al., 2020). Analyses of the internal structure of the Yellow River delta and its submarine Holocene equivalents indicate a rapid sea-level rise of 2–3 m at approximately 7.0 ka BP that pushes the shoreline 200 km westward (Liu et al., 2004). Farther south, pollen, algal, fungal spore, and microcharcoal data from the Neolithic Kuahuqiao site in the Lower Yangtze River indicate a rapid sea-level rise at 7.5 ka BP, inducing a marine transgression that inundates the site region, leading to the stoppage of early rice cultivation and abandonment of the site (Zong et al., 2007). This hypothesis seems to be confirmed by a recent study from the same area, which uses a rich data set of radiocarbon dates to reveal a sea-level rise of 2 m from 7.4 to 7.2 ka BP (Wang et al., 2012). The sea-level jump seems to coincide with the accelerated rise in the Hangzhou Bay (Xiong et al., 2020; Lyu et al., 2021) and widespread marine flooding across the Lake Taihu region (Zong et al., 2012). In Singapore, combining a high-resolution sea-level curve derived from 50 dates with the sedimentation rate, organic $\delta^{13}C$, and foraminiferal $\delta^{13}C$ indicates a sea-level rise of 3–5 m from 7.5 to 7.0 ka BP (Bird et al., 2007, 2010; Fig. 8d). A thick mangrove peat widely deposited over the Cambodian Mekong River lowlands is associated with the sea level rise at 7.5–7.0 ka BP (Tamura et al., 2009). In the Caribbean–Atlantic region, a study of the elevations and ages of drowned *Acropora palmata* reefs documents a catastrophic, meter-scale sea-level rise dated to 7.6 ka BP (Blanchon and Shaw, 1995; Blanchon et al., 2002).

Such a massive freshwater release influences sea water salinity and

density, which suppresses North Atlantic Deep Water convection and slows the Atlantic Meridional Overturning Circulation (AMOC) (Törnqvist and Hijma, 2012). In a core from the continental slope off northeastern Brazil, Arz et al. (2001) examine Ca intensities and the degree of preservation of the aragonitic shells of *Limacina inflata*, which are linked to the bottom-water corrosiveness, to infer a short-lived weakening of AMOC between 7.6 and 7.0 ka BP (Bakker et al., 2017). The universal climate anomaly modeled in response to the reduced AMOC is the cooling over the North Atlantic, which result in an increased latitudinal temperature gradient in favor of the development of stronger westerlies (Davis and Brewer, 2009). Strong westerlies would result in a northward shift of Atlantic storm tracks and higher precipitation over the northern latitudes of the eastern North Atlantic region, in contrast to reduced moisture penetration into the southern region (Fletcher et al., 2012; Magny et al., 2013). Convincing support for this interpretation is found in plentiful proxy records indicating a pattern of opposing precipitation variability, with dry conditions in the southwestern Mediterranean (Magny et al., 2011; Desprat et al., 2013; Fletcher et al., 2012) and wetter conditions over north-central Europe and in the northern Mediterranean between 7.6 and 7.0 ka BP (Haas et al., 1998; Magny, 2004; Magny et al., 2007). Other modeled changes include a southward migration of the Intertropical Convergence Zone, an increasingly El Niño-like state, and cooler temperatures throughout much of the northern hemisphere (Zhang and Delworth, 2005; Stríkis et al., 2011; Sun et al., 2011).

Overall, it is apparent that southward migration of the Intertropical Convergence Zone, onset of an increasingly El Niño-like state, reinforcement of the westerlies, and slowing of the AMOC develop between 7.6 and 7.0 ka BP as a consequence of changes in solar activity, volcanic activity, ice sheet dynamics, and summer insolation. Specifically solar activity influences the stratospheric ozone formation and induces a dramatic reorganization of the globally atmospheric circulation patterns (Haigh, 1996; Meehl et al., 2009). Additionally solar activity may trigger a reduction in North Atlantic Deep Water production (Goosse et al., 2002; Zhang and Delworth, 2005). Volcanic eruptions are well known to affect both shortwave and longwave radiation, producing a widespread cooling (Robock, 2000; Kobashi et al., 2017). The disturbance to the radiation also perturbs the globally atmospheric circulation (Fischer et al., 2007; Ridley et al., 2015). Massive freshwater release due to the retreat of the LIS influences sea water salinity and density, which suppresses North Atlantic Deep Water convection and slows the AMOC (Törnqvist and Hijma, 2012). The weakened AMOC transfers climate variability from the North Atlantic to the global scope via atmospheric teleconnections (Zhang and Delworth, 2005; Davis and Brewer, 2009). These factors couple with the gradually decreasing Northern Hemisphere summer insolation could explain the most robust features of the 7.2 ka climate event.

5. Conclusions

The 7.2 ka event is well represented in 58 paleoclimatic records from a variety of natural archives, including lake sediments, one loess section, speleothems, marine sediments, and ice cores across regions. As revealed by our synthesis results, proxy evidence clearly shows that the 7.2 ka event is characterized by a weaker Asian summer monsoon, and in contrast, a stronger South American summer monsoon. The event also involves strong cooling and wetter conditions in north-central Europe, widespread drying across Africa and the west-south North America, and contrasting patterns of precipitation change throughout the Mediterranean. Strong signals from polar ice core records reveal intensified atmospheric circulation and generally reduced temperatures. Despite varying climatic responses in different regions, a widely distributed signature for this event demonstrates that it is possibly of global significance.

These climate anomalies suggested by the proxy evidence reflect a southward migration of the Intertropical Convergence Zone, an increasing El Niño-like state, a reinforcement of the westerlies, and a slowing of the AMOC. Changes in these climate modes during 7.6–7.0 ka BP could have arisen because of the atmosphere–ocean–land feedback in response to an orbitally-induced decrease in summer solar insolation, large volcanic eruptions, reduction in solar activity, and meltwater flux into the North Atlantic.

It is noted that this review is in an early stage and gives only a preliminary analysis of the 7.2 ka event. As we have shown, the climate responses are rarely spatially uniform, and it remains exceedingly difficult to draw anomaly maps. Uncertainties remain concerning the spatial dimensions, duration, and magnitude of the climate event. Future advances will require more quantitative or semi-quantitative reconstructions and higher resolution records sampled at a higher spatial density to determine the complexity of the climate response. It is also important to develop significantly more research into assessments of potential transmission mechanisms and potential enhancements of natural feedback that amplify the relatively weak forcing related to fluctuations in solar output and volcanic eruptions.

There is increasing awareness and concern that anthropogenic activities may increase the risk of inducing abrupt climate changes in the earth system (Alley et al., 2003; Brovkin et al., 2021). However, most of state-of-the-art climate models seem to have been largely built for stability and unable to project abrupt climate changes (Valdes, 2011). The 7.2 ka event provides a better analog since it occurred during the Holocene Climate Maximum. Existing researches have shown that the 7.2 ka event may have impacted on ecosystem and human societies (Gronenborn, 2010; Wang et al., 2014). Future researches are thus in need to pay attention to its analogous role in undertraining the potential occurrence of abrupt climate change and its possible impact on ecosystems and human societies.

Declaration of Competing Interest

The authors declare that they have no conflict of interest.

Data availability

Data will be made available on request.

Acknowledgments

This work was jointly supported by the National Natural Science Foundation of China (Grants No.41888101 and No.41672176) and The Strategic Priority Research Program of the Chinese Academy of Sciences, Pan-Third Pole Environment Study for a Green Silk Road (Grant No. XDA20090000), Taiwan National Science and Technology Council (Grants 108-2410-H-002-199-MY2 and 111-2410-H-002-276-MY2).

Appendix A. Supplementary data

Supplementary data to this article can be found online at https://doi.org/10.1016/j.palaeo.2023.111525.

References

Alley, R.B., Ágústsdóttir, A.M., 2005. The 8 k event: Cause and consequences of a major Holocene abrupt climate change. Quat. Sci. Rev. 24, 1123–1149. https://doi.org/10.1016/j.quascirev.2004.12.004.

Alley, R.B., Marotzke, J., Nordhaus, W.D., Overpeck, J.T., Peteet, D.M., Pielke, R.A., Pierrehumbert, R.T., Rhines, P.B., Stocker, T.F., Talley, L.D., Wallace, J.M., 2003. Abrupt climate change. Science 299, 2005–2010. https://doi.org/10.1126/science.1081056.

Alley, R.B., Mayewski, P.A., Sowers, T., Stuiver, M., Taylor, K.C., Clark, P.U., 1997. Holocene climatic instability: a prominent, widespread event 8200 yr ago. Geology 25, 483–486. https://doi.org/10.1130/0091-7613(1997)025<0483:HCIAPW>2.3.CO;2.

Amorosi, A., Bruno, L., Campo, B., Morelli, A., Rossi, V., Scarponi, D., Hong, W., Bohacs, K.M., Drexler, T.M., 2017. Global sea-level control on local parasequence

architecture from the Holocene record of the Po Plain, Italy. Mar. Pet. Geol. 87, 99–111. https://doi.org/10.1016/j.marpetgeo.2017.01.020.
An, Z., Colman, S.M., Zhou, W., Li, X., Brown, E.T., Jull, A.J.T., Cai, Y., Huang, Y., Lu, X., Chang, H., Song, Y., Sun, Y., Xu, H., Liu, W., Jin, Z., Liu, X., Cheng, P., Liu, Y., Ai, L., Li, X., Liu, X., Yan, L., Shi, Z., Wang, X., Wu, F., Qiang, X., Dong, J., Lu, F., Xu, X., 2012. Interplay between the Westerlies and asian monsoon recorded in Lake Qinghai sediments since 32 ka. Sci. Rep. 2, 619. https://doi.org/10.1038/srep00619.
Arz, H.W., Gerhardt, S., Patzold, J., Rohl, U., 2001. Millennial-scale changes of surface- and deep-water flow in the western tropical Atlantic linked to Northern Hemisphere high-latitude climate during the Holocene. Geology 29, 239–242. https://doi.org/10.1130/0091-7613(2001)029<0239:MSCOSA>2.0.CO;2.
Asmerom, Y., Polyak, V., Burns, S., Rassmussen, J., 2007. Solar forcing of Holocene climate: New insights from a speleothem record, southwestern United States. Geology 35, 1–4. https://doi.org/10.1130/G22865A.1.
Aubán, J.B., Puchol, O.G., Barton, M., McClure, S., Gordó, S.P., 2016. Radiocarbon dates, climatic events, and social dynamics during the early Neolithic in Mediterranean Iberia. Quat. Int. 403, 201–210. https://doi.org/10.1016/j.quaint.2015.09.020.
Baker, P.A., Fritz, S.C., Garland, J., Ekdahl, E., 2005. Holocene hydrologic variation at Lake Titicaca, Bolivia/Peru, and its relationship to North Atlantic climate variation. J. Quat. Sci. 20, 655–662. https://doi.org/10.1002/jqs.987.
Bakker, P., Clark, P.U., Golledge, R.N., Schmittner, A., Weber, N.E., 2017. Centennial-scale Holocene climate variations amplified by Antarctic Ice Sheet discharge. Nature 541, 72–76. https://doi.org/10.1038/nature20582.
Bendle, J.A.P., Rosell-Mele, A., 2007. High-resolution alkenone sea surface temperature variability on the North Icelandic Shelf: implications for Nordic Seas palaeoclimatic development during the Holocene. The Holocene 17, 9–24. https://doi.org/10.1177/0959683607073269.
Berger, A., Loutre, M.F., 1991. Insolation values for the climate of the last 10 million years. Quat. Sci. Rev. 10, 297–317. https://doi.org/10.1016/0277-3791(91)90033-Q.
Berger, J.F., Delhon, C., Magnin, F., Bont, S., Peyric, D., Thiebault, S., Guilbert, R., Beeching, A., 2016. A fluvial record of the mid-Holocene rapid climatic changes in the middle Rhone valley (Espeluche-Lalo, France) and of their impact on late Mesolithic and early Neolithic societies. Quat. Sci. Rev. 136, 66–84. https://doi.org/10.1016/j.quascirev.2015.11.019.
Berkelhammer, M., Sinha, A., Stott, L., Cheng, H., Pausata, F., Yoshimura, K., 2012. An abrupt shift in the Indian Monsoon 4000 years Ago. Geophys. Res. Lett. 198, 75–87. https://doi.org/10.1029/2012GM001207.
Bernal, J.P., Cruz, F.W., Stríkis, N.M., Wang, X., Deininger, M., Catunda, M.C.A., Ortega-Obregón, C., Cheng, H., Edwards, R.L., Auler, A.S., 2016. High-resolution Holocene South American monsoon history recorded by a speleothem from Botuverá Cave, Brazil. Earth Planet Sci. Lett. 450, 186–196. https://doi.org/10.1016/j.epsl.2016.06.008.
Bird, M.I., Austin, W.E.N., Wurster, C.M., Fifield, L.K., Mojtahid, M., Sargeant, C., 2010. Punctuated eustatic sea-level rise in the early mid-Holocene. Geology 38, 803–806. https://doi.org/10.1130/G31066.1.
Bird, M.I., Fifield, L.K., The, T.S., Chang, C.H., Shirlaw, N., Lambeck, K., 2007. An inflection in the rate of early mid-Holocene eustatic sea-level rise: a new sea-level curve from Singapore. Estuar. Coast. Shelf Sci. 71, 523–536. https://doi.org/10.1016/j.ecss.2006.07.004.
Blunier, T., Chappellaz, J., Schwander, J., Stauffer, B., Raynaud, D., 1995. Variations in atmospheric methane concentration during the Holocene epoch. Nature 374, 46–49. https://doi.org/10.1038/374046a0.
Blanchon, P., Jones, B., Ford, D.C., 2002. Discovery of a submerged relic reef and shoreline off Grand Cayman: further support for an early Holocene jump in sea level. Sediment. Geol. 147, 253–270. https://doi.org/10.1016/S0037-0738(01)00143-9.
Blanchon, P., Shaw, J., 1995. Reef drowning during the last deglaciation: evidence for catastrophic sea-level rise and ice-sheet collapse. Geology 23, 4–8. https://doi.org/10.1130/0091-7613(1995)023<0004:RDDTLD>2.3.CO;2.
Bond, G., Showers, W., Cheseby, M., Lotti, R., Almasi, P., Demenocal, P., Priore, P., Cullen, H., Hajdas, I., Bonani, G., 1997. A pervasive millennial-scale cycle in North Atlantic Holocene and glacial climates. Science 278, 1257–1266. https://doi.org/10.1126/science.278.5341.1257.
Bond, G., Kromer, B., Beer, J., Muscheler, R., Evans, M.N., Showers, W., Hoffmann, S., Lotti-Bond, R., Hajdas, I., Bonani, G., 2001. Persistent solar influence on North Atlantic climate during the Holocene. Science 294, 2130–2136. https://www.jstor.org/stable/3085350.
Brooks, N., 2006. Cultural responses to aridity in the Middle Holocene and increased social complexity. Quat. Int. 151, 29–49. https://doi.org/10.1016/j.quaint.2006.01.013.
Brovkin, V., Brook, E., Williams, J.W., Bathiany, S., Lenton, T.M., Barton, M., DeConto, R.M., Donges, J.F., Ganopolski, A., McManus, J., Praetorius, S., de Vernal, A., Abe-Ouchi, A., Cheng, H., Claussen, M., Crucifix, M., Gallopín, G., Iglesias, V., Kaufman, D.S., Kleinen, T., Lambert, F., van der Leeuw, S., Liddy, H., Loutre, M.F., McGee, D., Rehfeld, K., Rhodes, R., Seddon, A.W.R., Trauth, M.H., Vanderveken, L., Yu, Z., 2021. Past abrupt changes, tipping points and cascading impacts in the Earth system. Nat. Geosci. 14, 550–558. https://doi.org/10.1038/s41561-021-00790-5.
Bruno, L., Bohacs, K.M., Campo, B., Drexler, T.M., Rossi, V., Sammartino, I., Scarponi, D., Hong, W., Amorosi, A., 2017. Early Holocene transgressive palaeogeography in the Po coastal plain (northern Italy). Sedimentology 64, 1792–1816. https://doi.org/10.1111/sed.12374.
Cai, Y., Cheng, X., Ma, L., Mao, R., Breitenbach, S.F.M., Zhang, H., Xue, G., Cheng, H., Edwards, R.L., An, Z., 2021. Holocene variability of East asian summer monsoon as viewed from the speleothem δ18O records in Central China. Earth Planet. Sci. Lett. 558, 116758 https://doi.org/10.1016/j.epsl.2021.116758.
Cai, Y., Zhang, H., Cheng, H., An, Z., Edwards, R.L., Wang, X., Tan, L., Liang, F., Wang, J., Kelly, M., 2012. The Holocene indian monsoon variability over the southern Tibetan Plateau and its teleconnections. Earth Planet. Sci. Lett. 335–336, 135–144. https://doi.org/10.1016/j.epsl.2012.04.035.
Carlson, A.E., Legrande, A.N., Oppo, D.W., Came, R.E., Schmidt, G.A., Anslow, F.S., Licciardi, J.M., Obbink, E.A., 2008. Rapid early Holocene deglaciation of the Laurentide ice sheet. Nat. Geosci. 1, 620–624. https://doi.org/10.1038/ngeo285.
Cheng, H., Sinha, A., Verheyden, S., Nader, F.H., Li, X.L., Zhang, P.Z., Yin, J.J., Yi, L., Peng, Y.B., Rao, Z.G., Ning, Y.F., Edwards, R.L., 2015. The climate variability in northern Levant over the past 20,000 years. Geophys. Res. Lett. 42, 8641–8650. https://doi.org/10.1002/2015GL065397.
Cole, J.M., Goldstein, S.L., deMenocal, P.B., Hemming, S.R., Grousset, F.E., 2009. Contrasting compositions of Saharan dust in the eastern Atlantic Ocean during the last deglaciation and African Humid Period. Earth Planet. Sci. Lett. 278, 257–266. https://doi.org/10.1016/j.epsl.2008.12.011.
Dansgaard, W., Johnsen, S.J., Clausen, H.B., Dahl-Jensen, D., Gundestrup, N.S., Hammer, C.U., Hvidberg, C.S., Steffensen, J.P., Sveinbjörnsdottir, A.E., Jouzel, J., Bond, G., 1993. Evidence for general instability of past climate from a 250-kyr ice-core record. Nature 364, 218–220. https://doi.org/10.1038/364218a0.
Davis, B.A.S., Brewer, S., 2009. Orbital forcing and role of the latitudinal insolation/temperature gradient. Clim. Dyn. 32, 143–165. https://doi.org/10.1007/s00382-008-0480-9.
deMenocal, P., Ortiz, J., Guilderson, T., Adkins, J., Sarnthein, M., Baker, L., Yarusinsky, M., 2000. Abrupt onset and termination of the African Humid Period: rapid climate responses to gradual insolation forcing. Quat. Sci. Rev. 19, 347–361. https://doi.org/10.1016/S0277-3791(99)00081-5.
Desprat, S., Combourieu-Nebout, N., Essallami, L., Sicre, M.A., Dormoy, I., Peyron, O., Siani, G., Roumazeilles, V.B., Turon, J.L., 2013. Deglacial and Holocene vegetation and climatic changes in the southern Central Mediterranean from a direct land–sea correlation. Clim. Past 9 (767–787), 2013. https://doi.org/10.5194/cp-9-767-2013.
Dong, G., 2013. Neolithic cultural evolution and its environmental driving force in Gansu-Qinghai region problems and perspectives. Mar. Geol. Quat. Geol. 33, 67–75 (in Chinese with English abstract).
Dyke, A.S., Moore, A., Robinson, L., 2003. Deglaciation of North America. Geological Survey of Canada, Ottawa. Tech. Rep. Open File 1574.
Ersek, V., Clark, P.U., Mix, A.C., Cheng, H., Edwards, R.L., 2012. Holocene winter climate variability in mid-latitude western North America. Nat. Commun. 3, 1219. https://doi.org/10.1038/ncomms2222.
Feng, X., Yang, Y., Cheng, H., Zhao, J., Kong, X., Zhang, P., He, Z., Shi, X., Edwards, R.L., 2019. The 7.2 ka climate event: Evidence from high-resolution stable isotopes and trace element records of stalagmite in Shuiming Cave, Chongqing, China. Holocene 30, 145–154. https://doi.org/10.1177/0959683619875809.
Filippidi, A., Triantaphyllou, M.V., Lange, G.J.D., 2016. Eastern-Mediterranean ventilation variability during sapropel S1 formation, evaluated at two sites influenced by deep-water formation from Adriatic and Aegean Seas. Quat. Sci. Rev. 144, 95–106. https://doi.org/10.1016/j.quascirev.2016.05.024.
Fischer, E.M., Luterbacher, J., Zorita, E., Tett, S.F.B., Casty, C., Wanner, H., 2007. European climate response to tropical volcanic eruptions over the last half millennium. Geophys. Res. Lett. 34, L05707. https://doi.org/10.1029/2006GL027992.
Fleitmann, D., Burns, S.J., Mudelsee, M., Neff, U., Kramers, J., Mangini, A., Matter, A., 2003. Holocene forcing of the Indian Monsoon recorded in a stalagmite from southern Oman. Science 300, 1737–1739. https://doi.org/10.1126/science.1083130.
Fletcher, W.J., Debret, M., Goñi, M.F.S., 2012. Mid-Holocene emergence of a lowfrequency millennial oscillation in western Mediterranean climate: Implications for past dynamics of the North Atlantic atmospheric westerlies. The Holocene 23, 153–166. https://doi.org/10.1177/0959683612460783.
Frisia, S., Borsato, A., Mangini, A., Spötl, C., Madonia, G., Sauro, U., 2006. Holocene climate variability in Sicily from a discontinuous stalagmite record and the Mesolithic to Neolithic transition. Quat. Res. 66, 388–400. https://doi.org/10.1016/j.yqres.2006.05.003.
Goosse, H., Renseen, H., Selten, F.M., Haarsma, R.J., Opsteegh, J.D., 2002. Potential causes of abrupt climate events: a numerical study with a three-dimensional climate model. Geophys. Res. Lett. 29, 1860. https://doi.org/10.1029/2002GL014993.
Gray, L.J., Beer, J., Geller, M., Haigh, J.D., Lockwood, M., Matthes, K., Cubasch, U., Fleitmann, D., Harrison, G., Hood, L., Luterbacher, J., Meehl, G.A., Shindell, D., van Geel, B., White, W., 2010. Solar influences on climate. Rev. Geophys. 48, RG4001. https://doi.org/10.1029/2009RG000282.
Gronenborn, D., 2010. Climate, crises and the neolithisation of Central Europe between IRD-events 6 and 4. In: Gronenborn, D., Petrasch, J. (Eds.), The Spread of the Neolithic to Central Europe. Verlag des Romisch-Germanischen Zentralmuseums, Mainz, pp. 61–80.
Gupta, A.K., Das, M., Anderson, D.M., 2005. Solar influence on the indian summer monsoon during the Holocene. Geophys. Res. Lett. 32, L17703. https://doi.org/10.1029/2005GL022685.
Haas, J.N., Richoz, I., Tinner, W., Wick, L., 1998. Synchronous Holocene climatic oscillations recorded on the Swiss Plateau and at timberline in the Alps. The Holocene 8, 301–309. https://doi.org/10.1191/095968398675491173.
Haigh, J.D., 1996. The impact of solar variability on climate. Science 272, 981–984. https://doi.org/10.1126/science.272.5264.9.
Haug, G.H., Hughen, K.A., Sigman, D.M., Peterson, L.C., Röhl, U., 2001. Southward migration of the Intertropical Convergence Zone through the Holocene. Science 293, 1304–1308. https://doi.org/10.1126/science.1059725.

Herrle, J.O., Bollmann, J., Gebühr, C., Schulz, H., Sheward, R.M., Giesenberg, A., 2018. Black Sea outfow response to Holocene meltwater events. Sci. Rep. 8, 4081. https://doi.org/10.1038/s41598-018-22453-z.
Hou, M., Wu, W., 2021. A review of 6000–5000 cal BP climatic anomalies in China. Quat. Int. 571, 58–72.
Huang, C., Rao, Z., Li, Y., Yang, W., Liu, L., Zhang, X., Wu, Y., 2020. Holocene summer temperature in arid Central Asia linked to millennial-scale North Atlantic climate events and driven by centennial-scale solar activity. Palaeogeogr. Palaeoclimatol. Palaeoecol. 556, 109880 https://doi.org/10.1016/j.palaeo.2020.109880.
Hughes, P.D.M., Blundell, A., Charman, D.J., Bartlett, S., Daniell, J.R.G., Wojatschke, A., Chambers, F.M., 2006. An 8500 cal. Year multi-proxy climate record from a bog in eastern Newfoundland: contributions of meltwater discharge and solar forcing. Quat. Sci. Rev. 25, 1208–1227. https://doi.org/10.1016/j.quascirev.2005.11.001.
IPCC, 2021. Climate Change 2021: The Physical Science Basis. Contribution of Working Group I to the Sixth Assessment Report of the Intergovernmental Panel on Climate Change [Masson-Delmotte. Cambridge University Press, Cambridge, United Kingdom and New York, pp. 2391–pp.
Jansson, K.N., Kleman, J., 2004. Early Holocene glacial lake meltwater injections into the Labrador Sea and Ungava Bay. Paleoceanography 19, PA1001.
Karlén, W., 1988. Scandinavian glacial and climatic fluctuations during the Holocene. Quat. Sci. Rev. 7, 199–209. https://doi.org/10.1016/0277-3791(88)90006-6.
Kobashi, T., Menviel, L., Thömmes, A.J., Vinther, B.M., Box, J.E., Muscheler, R., Nakaegawa, T., Pfister, P.L., Döring, M., Leuenberger, M., Wanner, H., Ohmura, A., 2017. Volcanic influence on centennial to millennial Holocene Greenland temperature change. Sci. Rep. 7, 1441. https://doi.org/10.1038/s41598-017-01451-7.
Korhola, A., Weckström, J., Holmström, L., Erästö, P., 2000. A Quantitative Holocene Climatic Record from Diatoms in Northern Fennoscandia. Quat. Res. 54, 284–294. https://doi.org/10.1006/qres.2000.2153.
Kubota, Y., Kimoto, K., Tada, R., Oda, H., Yokoyama, Y., Matsuzaki, H., 2010. Variations of East asian summer monsoon since the last deglaciation based on Mg/Ca and oxygen isotope of planktic foraminifera in the northern East China Sea. Paleoceanogr. Paleoclimatol. 25, PA4205. https://doi.org/10.1029/2009PA001891.
Li, D., Yu, M., Jia, Y., Steinke, S., Li, L., Xiang, R., Zhao, M., 2021a. Gradually cooling of the Yellow Sea warm current driven by tropical Pacific subsurface water temperature changes over the past 5 kyr. Geophys. Res. Lett. 48, e2021GL093534 https://doi.org/10.1029/2021GL093534.
Li, Y., Han, L., Liu, X., Song, Y., Wang, Y., 2021b. Correlation and anti-correlation of the asian summer monsoon and westerlies during the Holocene. Gondwana Res. 91, 112–120. https://doi.org/10.1016/j.gr.2020.12.013.
Liu, D., Wang, Y., Cheng, H., Edwards, R.L., Kong, X., 2015. Cyclic changes of asian monsoon intensity during the early mid-Holocene from annually-laminated stalagmites, Central China. Quat. Sci. Rev. 121, 1–10. https://doi.org/10.1016/j.quascirev.2015.05.003.
Liu, J.P., Milliman, J.D., Gao, S., Cheng, P., 2004. Holocene development of the Yellow River's subaqueous delta, North Yellow Sea. Mar. Geol. 209, 45–67. https://doi.org/10.1016/j.margeo.2004.06.009.
Liu, L., Xu, L., Guan, H., Sun, Z., Wang, L., Mao, S., Liu, L., Wu, N., 2020a. The source of glycerol dibiphytanyl glycerol tetraethers and temperature reconstruction since 8.2 ka in the Central Okinawa Trough. J. Trop. Oceanogr. 39, 77–92 (in Chinese with English abstract).
Liu, X., Rao, Z., Shen, C., Chen, J., Chen, S., Wang, F., Chen, F., 2019. Holocene Solar activity Imprint on Centennial- to Multidecadal-Scale Hydroclimatic Oscillations in Arid Central Asia. J. Geophys. Res. Atmos. 124, 2562–2573. https://doi.org/10.1029/2018JD029699.
Liu, X., Sun, Y., Vandenberghe, J., Cheng, P., Zhang, X., Gowan, E.J., Lohmann, G., An, Z., 2020b. Centennial- to millennial-scale monsoon changes since the last deglaciation linked to solar activities and North Atlantic cooling. Clim. Past 16 (315–324), 2020. https://doi.org/10.5194/cp-16-315-2020.
Liu, Y., Henderson, G.M., Hu, C., Mason, A.J., Charnley, N., Johnson, K.R., Xie, S., 2013. Links between the East asian monsoon and North Atlantic climate during the 8,200 year event. Nat. Geosci. 6, 117–120. https://doi.org/10.1038/ngeo1708.
Lü, H., Zhang, J., 2008. Neolithic cultural evolution and Holocene climate change in the Guanzhong Basin, Shanxi, China. Quat. Sci. 28, 1050–1060 (in Chinese with English abstract).
Lyu, Y., Tong, C., Saito, Y., Meadows, E., Wang, Z., 2021. Early to mid-Holocene sedimentary evolution on the southeastern coast of Hangzhou Bay, East China, in response to sea-level change. Mar. Geol. 442, 106655 https://doi.org/10.1016/j.margeo.2021.106655.
Machida, H., 1999. The stratigraphy, chronology and distribution of distal marker-tephras in and around Japan. Glob. Planet. Change 21, 71–94. https://doi.org/10.1016/S0921-8181(99)00008-9.
Magny, M., 2004. Holocene climate variability as reflected by mid-european lake-level fluctuations and its probable impact on prehistoric human settlements. Quat. Int. 113, 65–79. https://doi.org/10.1016/S1040-6182(03)00080-6.
Magny, M., de Beaulieu, J.L., Drescher-Schneider, R., Vannière, B., Walter-Simonnet, A. V., Miras, Y., Millet, L., Bossuet, G., Peyron, O., Brugiapaglia, E., Leroux, A., 2007. Holocene climate changes in the Central Mediterranean as recorded by Lake-level fluctuations at Lake Accesa (Tuscany, Italy). Quat. Sci. Rev. 26, 1736–1758. https://doi.org/10.1016/j.quascirev.2007.04.014.
Magny, M., Joannin, S., Galop, D., Vannière, B., Haas, J.N., Bassetti, M., Bellintani, P., Scandolari, R., Desmet, M., 2012. Holocene palaeohydrological changes in the northern Mediterranean borderlands as reflected by the Lake-level record of Lake Ledro, northeastern Italy. Quat. Res. 77, 382–396. https://doi.org/10.1016/j.yqres.2012.01.005.
Magny, M., Combourieu-Nebout, N., de Beaulieu, J.L., Bout-Roumazeilles, V., Colombaroli, D., Desprat, S., Francke, A., Joannin, S., Ortu, E., Peyron, O., Revel, M., Sadori, L., Siani, G., Sicre, M.A., Samartin, S., Simonneau, A., Tinner, W., Vannière, B., Wagner, B., Zanchetta, G., Anselmetti, F., Brugiapaglia, E., Chapron, E., Debret, M., Desmet, M., Didier, J., Essallami, L., Galop, D., Gilli, A., Haas, J.N., Kallel, N., Millet, L., Stock, A., Turon, J.L., Wirth, S., 2013. North-south palaeohydrological contrasts in the Central Mediterranean during the Holocene: tentative synthesis and working hypotheses. Clim. Past 9, 2043–2071. https://doi.org/10.5194/cp-9-2043-2013.
Magny, M., Vannière, B., Calo, C., Millet, L., Leroux, A., Peyron, O., Zanchetta, G., La Mantia, T., Tinner, W., 2011. Holocene hydrological changes in south-western Mediterranean as recorded by lake-level fluctuations at Lago Preola, a coastal lake in southern Sicily, Italy. Quat. Sci. Rev. 30, 2459–2475. https://doi.org/10.1016/j.quascirev.2011.05.018.
Man, W., Zhou, T., Jungclaus, J.H., 2014. Effects of large volcanic eruptions on global summer climate and East Asian Monsoon changes during the last millennium: analysis of MPI-ESM simulations. J. Clim. 27, 7394–7409. https://doi.org/10.1175/JCLI-D-13-00739.1.
Marchitto, T.M., Muscheler, R., Ortiz, J.D., Carriquiry, J.D., van Geen, A., 2010. Dynamical response of the tropical Pacific Ocean to solar forcing during the early Holocene. Science 330, 1378–1381. https://doi.org/10.1126/science.1194887.
Mayewski, P.A., Meeker, L.D., Twickler, M.S., Whitlow, S., Yang, Q., Lyons, W.B., Prentice, M., 1997. Major features and forcing of high-latitude northern hemisphere atmospheric circulation using a 110,000-year-long glaciochemical series. J. Geophys. Res. Oceans 102, 26345–26366. https://doi.org/10.1029/96JC03365.
Mayewski, P.A., Rohling, E.E., Stager, J.C., Karlén, W., Maasch, K.A., Meeker, L.D., Meyerson, E.A., Gasse, F., van Kreveld, S., Holmgren, K., Lee-Thorp, J., Rosqvist, G., Rack, F., Staubwasser, M., Schneider, R.R., Steig, E.J., 2004. Holocene climate variability. Quat. Res. 62, 243–255. https://doi.org/10.1016/j.yqres.2004.07.001.
Meehl, G.A., Arblaster, J.M., Matthes, K., Sassi, F., van Loon, H., 2009. Amplifying the Pacific climate System Response to a small 11-Year Solar Cycle Forcing. Nature 325, 1114–1118. https://doi.org/10.1126/science.1172872.
Menounos, B., Osborn, G., Clague, J.J., Luckman, B.H., 2009. Latest Pleistocene and Holocene glacier fluctuations in western Canada. Quat. Sci. Rev. 28, 2049–2074. https://doi.org/10.1016/j.quascirev.2008.10.018.
Menounos, B., Clague, J.J., Osborn, G., Davis, P.T., Ponce, F., Goehring, B., Maurer, M., Rabassa, J., Coronato, A., Marr, R., 2013. Latest Pleistocene and Holocene glacier fluctuations in southernmost Tierra del Fuego, Argentina. Quat. Sci. Rev. 77, 70–79. https://doi.org/10.1016/j.quascirev.2013.07.008.
Miller, G.H., Geirsdóttir, A., Zhong, Y., Larsen, D.J., Otto-Bliesner, B.L., Holland, M.M., Bailey, D.A., Refsnider, K.A., Lehman, S.J., Southon, J.R., Anderson, C., Björnsson, H., Thordarson, T., 2012. Abrupt onset of the Little Ice Age triggered by volcanism and sustained by sea-ice/ocean feedbacks. Geophys. Res. Lett. 39, L02708. https://doi.org/10.1029/2011GL050168.
Munz, P.M., Steinke, S., Böll, A., Lückge, A., Groeneveld, J., Kucera, M., Schulz, H., 2017. Decadal resolution record of Oman upwelling indicates solar forcing of the indian summer monsoon (9–6 ka). Clim. Past 13, 491–509. https://doi.org/10.5194/cp-13-491-2017.
Nan, Q., Li, T., Chen, J., Chang, F., Yu, X., Xu, Z., Pi, Z., 2017. Holocene paleoenvironment changes in the northern Yellow Sea: evidence from alkenone-derived sea surface temperature. Palaeogeogr. Palaeoclimatol. Palaeoecol. 483, 83–93. https://doi.org/10.1016/j.palaeo.2017.01.031.
National Research Council, 2002. Abrupt Climate Change: Inevitable Surprises. National Academy Press, Washington, DC.
Neff, U., Burns, S.J., Mangini, A., Mudelsee, M., Fleitmann, D., Matter, A., 2001. Strong coherence between solar variability and the monsoon in Oman between 9 and 6 kyr ago. Nature 411, 290–293. https://doi.org/10.1038/35077048.
Nesje, A., 2009. Latest Pleistocene and Holocene alpine glacier fluctuations in Scandinavia. Quat. Sci. Rev. 28, 2119–2136. https://doi.org/10.1016/j.quascirev.2008.12.016.
Ning, D., Zhang, E., Sun, W., Chang, J., Shulmeister, J., 2017. Holocene Indian Summer Monsoon variation inferred from geochemical and grain size records from Lake Ximenglongtan, southwestern China. Palaeogeogr. Palaeoclimatol. Palaeoecol. 487, 260–269. https://doi.org/10.1016/j.palaeo.2017.09.008.
O'Brien, S.R., Mayewski, P.A., Meeker, L.D., Meese, D.A., Twickler, M.S., Whitlow, S.I., 1995. Complexity of Holocene climate as Reconstructed from a Greenland Ice Core. Science 270, 1962–1964.
Pędziszewska, A., Tylmann, W., Witak, M., Piotrowska, N., Maciejewska, E., Latałowa, M., 2015. Holocene environmental changes reflected by pollen, diatoms, and geochemistry of annually laminated sediments of Lake Suminko in the Kashubian Lake District (N Poland). Rev. Palaeobot. Palynol. 216, 55–75. https://doi.org/10.1016/j.revpalbo.2015.01.008.
Pérez-Rodríguez, M., Gilfedder, B.S., Hermanns, Y.M., Biester, H., 2016. Solar output Controls Periodicity in Lake Productivity and Wetness at Southernmost South America. Sci. Rep. 6, 37521. https://doi.org/10.1038/srep37521.
Ramos-Román, M.J., Jiménez-Moreno, G., Camuera, J., García-Alix, A., Anderson, R.S., Jimenez-Espejo, F.J., Sachse, D., Toney, J.L., Carrión, J.S., Webster, C., Yanes, Y., 2018. Millennial-scale cyclical environment and climate variability during the Holocene in the western Mediterranean region deduced from a new multiproxy analysis from the Padul record (Sierra Nevada, Spain). Glob. Planet. Change 168, 35–53. https://doi.org/10.1016/j.gloplacha.2018.06.003.
Rasmussen, S.O., Seierstad, I.K., Andersen, K.K., Bigler, M., Dahl-Jensen, D., Johnsen, S. J., 2008. Synchronization of the NGRIP, GRIP, and GISP2 ice cores across MIS 2 and palaeoclimatic implications. Quat. Sci. Rev. 27, 18–28. https://doi.org/10.1016/j.quascirev.2007.01.016.

Rasmussen, T.L., Thomsen, E., 2010. Holocene temperature and salinity variability of the Atlantic Water inflow to the Nordic seas. The Holocene 20, 1223–1234. https://doi.org/10.1177/0959683610371996.
Renssen, H., Goosse, H., Muscheler, R., 2006. Coupled climate model simulation of Holocene cooling events: oceanic feedback amplifies solar forcing. Clim. Past 2, 79–90. https://doi.org/10.5194/cp-2-79-2006.
Revel, M., Ducassou, E., Grousset, F.E., Bernasconi, S.M., Migeon, S., Revillon, S., Mascle, J., Murat, A., Zaragosi, S., Bosch, D., 2010. 100,000 years of african monsoon variability recorded in sediments of the Nile margin. Quat. Sci. Rev. 29, 1342–1362. https://doi.org/10.1016/j.quascirev.2010.02.006.
Ridley, H.E., Asmerom, Y., Baldini, J.U.L., Breitenbach, S.F.M., Aquino, V.V., Prufer, K. M., Culleton, B.J., Polyak, V., Lechleitner, F.A., Kennett, D.J., Zhang, M., Marwan, N., Macpherson, C.G., Baldini, L.M., Xiao, T., Peterkin, J.L., Awe, J., Haug, G.H., 2015. Aerosol forcing of the position of the intertropical convergence zone since AD 1550. Nat. Geosci. 8, 195–200. https://doi.org/10.1038/ngeo2353.
Roberts, N., Eastwood, W.J., Kuzucuoglu, C., Fiorentino, G., Caracuta, V., 2011. Climatic, vegetation and cultural change in the eastern Mediterranean during the mid-Holocene environmental transition. The Holocene 21, 147–162. https://doi.org/10.1177/0959683610386819.
Robock, A., 2000. Volcanic eruptions and climate. Rev. Geophys. 38, 191–219. https://doi.org/10.1029/1998RG000054.
Ryder, J.M., Thomson, B., 1986. Neoglaciation in the southern Coast Mountains of British Columbia: chronology prior to the late Neoglacial maximum. Can. J. Earth Sci. 23, 273–287. https://doi.org/10.1139/e86-031.
Sagawa, T., Kuwae, M., Tsuruoka, K., Nakamura, Y., Ikehara, M., Murayama, M., 2014. Solar forcing of centennial-scale East asian winter monsoon variability in the mid- to late Holocene. Earth Planet. Sci. Lett. 395, 124–135. https://doi.org/10.1016/j.epsl.2014.03.043.
Sánchez, M.C., Espejo, F.J.J., Vallejo, M.D.S., Gibaja Bao, J.F., Carvalho, A.F., Martinez-Ruiz, F., Gamiz, M.R., Flores, J.A., Paytan, A., López Sáez, J.A., Peña-Chocarro, L., Carrión, J.S., Muñiz, A.M., Izquierdo, E.R., Cantal, J.A.R., Dean, R.M., Salgueiro, E., Sánchez, R.M.M., de Gracia, J.J.D.R., Francisco, M.C.L., Peláez, J.L.V., Rodríguez, L. L., Bicho, N.F., 2012. The Mesolithic-Neolithic transition in southern Iberia. Quat. Res. 77, 221–234. https://doi.org/10.1016/j.yqres.2011.12.003.
Schmidt, M.W., Weinlein, W.A., Marcantonio, F., Lynch-Stieglitz, J., 2012. Solar forcing of Florida Straits surface salinity during the early Holocene. Paleoceanography 27, PA3204. https://doi.org/10.1029/2012PA002284.
Shuman, B., 2012. Patterns, processes, and impacts of abrupt climate change in a warm world: the past 11,700 years. WIREs Clim. Change 3, 19–43. https://doi.org/10.1002/wcc.152.
Shuman, B.N., Marsicek, J., 2016. The structure of Holocene climate change in mid-latitude North America. Quat. Sci. Rev. 141, 38–51. https://doi.org/10.1016/j.quascirev.2016.03.009.
Siani, W., Magny, M., Paterne, M., Debret, M., Fontugne, M., 2013. Paleohydrology reconstruction and Holocene climate variability in the South Adriatic Sea. Clim. Past 9, 499–515. https://doi.org/10.5194/cp-9-499-2013.
Sigl, M., Winstrup, M., McConnell, J.R., Welten, K.C., Plunkett, G., Ludlow, F., Büntgen, U., Caffee, M., Chellman, N., Dahl-Jensen, D., Fischer, H., Kipfstuhl, S., Kostick, C., Maselli, O.J., Mekhaldi, F., Mulvaney, R., Muscheler, R., Pasteris, D.R., Pilcher, J.R., Salzer, M., Schüpbach, S., Steffensen, J.P., Vinther, B.M., Woodruff, T. E., 2015. Timing and climate forcing of volcanic eruptions for the past 2,500 years. Nature 523, 543–549. https://doi.org/10.1038/nature14565.
Smith, V.C., Staff, R.A., Blockley, S.P.E., Ramsey, C.B., Nakagawa, T., Mark, D.F., Takemura, K., Danhara, T., Suigetsu 2006 Project Members, 2013. Identification and correlation of visible tephras in the Lake Suigetsu SG06 sedimentary archive, Japan: chronostratigraphic markers for synchronising of east Asian/west Pacific palaeoclimatic records across the last 150 ka. Quat. Sci. Rev. 67, 121–137. https://doi.org/10.1016/j.quascirev.2013.01.026.
Steig, E.J., Morse, D.L., Waddington, E.D., Stuiver, M., Grootes, P.M., Mayewski, P.A., Twickler, M.S., Whitlow, S.I., 2000. Wisconsinan and Holocene climate history from an ice core at Taylor Dome, Western Ross Embayment, Antarctica. Geogr. Ann. 82 A, 213–235. https://doi.org/10.1111/j.0435-3676.2000.00122.x.
Steinhilber, F., Abreu, J.A., Beer, J., Wilhelms, F., 2009. 9,400 years of cosmic radiation and solar activity from ice cores and tree rings. Proc. Natl. Acad. Sci. U. S. A. 109, 5967–5971. https://doi.org/10.1073/pnas.1118965109.
Stríkis, N.M., Cruz, F.W., Cheng, H., Karmann, I., Edwards, R.L., Vuille, M., Wang, X., de Paula, M.S., Novello, V.F., Auler, A.S., 2011. Abrupt variations in south american monsoon rainfall during the Holocene based on a speleothem record from Central-Eastern Brazil. Geology 39, 1075–1078. https://doi.org/10.1130/G32098.1.
Stuiver, M., Reimer, P.J., Braziunas, T.F., 1998. High-Precision radiocarbon age calibration for terrestrial and marine samples. Radiocarbon 40, 1127–1151. https://doi.org/10.1017/S0033822200019172.
Stuiver, M., Braziunas, T.F., Grootes, P.M., Zielinski, G.A., 1997. Is there evidence for Solar Forcing of climate in the GISP2 Oxygen Isotope Record? Quat. Res. 48, 259–266. https://doi.org/10.1006/qres.1997.1931.
Sun, Y., Clemens, S.C., Morrill, C., Lin, X., Wang, X., An, Z., 2011. Influence of Atlantic meridional overturning circulation on the East asian winter monsoon. Nat. Geosci. 5, 46–49. https://doi.org/10.1038/ngeo1326.
Surić, M., Columbu, A., Lončarić, R., Bajo, P., Bočić, N., Lončar, N., Drysdale, R.N., Hellstrom, J.C., 2021. Holocene hydroclimate changes in continental Croatia recorded in speleothem δ13C and δ18O from Nova Grgosova Cave. The Holocene 31, 1401–1416. https://doi.org/10.1177/09596836211019120.
Tamura, T., Saito, Y., Sieng, S., Ben, B., Kong, M., Sim, I., Choup, S., Akiba, F., 2009. Initiation of the Mekong River delta at 8 ka: evidence from the sedimentary succession in the cambodian lowland. Quat. Sci. Rev. 28, 327–344. https://doi.org/10.1016/j.quascirev.2008.10.010.
Tesi, T., Asioli, A., Minisini, D., Maselli, V., Valle, G.D., Gamberi, F., Langone, L., Cattaneo, A., Montagna, P., Trincardi, F., 2017. Large-scale response of the Eastern Mediterranean thermohaline circulation to african monsoon intensification during sapropel S1 formation. Quat. Sci. Rev. 159, 139–154. https://doi.org/10.1016/j.quascirev.2017.01.020.
Thompson, L.G., Mosley-Thompson, E., Davis, M.E., Henderson, K.A., Brecher, H.H., Zagorodnov, V.S., Mashiotta, T.A., Lin, P., Mikhalenko, V.N., Hardy, D.R., Beer, J., 2002. Kilimanjaro ice core records: evidence of Holocene climate change in Tropical Africa. Science 298, 589–593. https://doi.org/10.1126/science.1073198.
Törnqvist, T.E., Hijma, M.P., 2012. Links between early Holocene ice-sheet decay, sea-level rise and abrupt climate change. Nat. Geosci. 5, 601–606. https://doi.org/10.1038/ngeo1536.
Ullman, D., Carlson, A.E., Hostetler, S.W., Clark, P.U., Cuzzone, J., Milne, G.A., Winsor, K., Caffee, M., 2016. Final Laurentide ice-sheet deglaciation and Holocene climate-sea level change. Quat. Sci. Rev. 152, 49–59. https://doi.org/10.1016/j.quascirev.2016.09.014.
Valdes, P., 2011. Built for stability. Nat. Geosci. 4, 414–416. https://doi.org/10.1038/ngeo1200.
Viau, A.E., Gajewski, K., Sawada, M.C., Fines, P., 2006. Millennial-scale temperature variations in North America during the Holocene. J. Geophys. Res. 111, D09102. https://doi.org/10.1029/2005JD006031.
Vinther, B.M., Clausen, H.B., Johnsen, S.J., Rasmussen, S.O., Andersen, K.K., Buchardt, S. L., Dahl-Jensen, D., Seierstad, I.K., Siggaard-Andersen, M.L., Steffensen, J.P., Svensson, A., Olsen, J., Heinemeier, J., 2006. A synchronized dating of three Greenland ice cores throughout the Holocene. J. Geophys. Res. Atmos. 111, D13102. https://doi.org/10.1029/2005JD006921.
Wang, C., Lu, H., Zhang, J., Gu, Z., He, K., 2014. Prehistoric demographic fluctions in China inferred from radiocarbon data and their linkage with climate change over the past 50000 years. Quat. Sci. Rev. 98, 45–59. https://doi.org/10.1016/j.quascirev.2014.05.015.
Wang, Y., Cheng, H., Edwards, R.L., He, Y., Kong, X., An, Z., Wu, J., Kelly, M.J., Dykoski, C.A., Li, X., 2005. The Holocene Asian Monsoon: Links to solar changes and North Atlantic climate. Science 308, 854–857. https://doi.org/10.1126/science.1106296.
Wang, Z., Zhuang, C., Saito, Y., Chen, J., Zhan, Q., Wang, X., 2012. Early mid-Holocene Sea-level change and coastal environmental response on the southern Yangtze delta plain, China: implications for the rise of Neolithic culture. Quat. Sci. Rev. 35, 51–62. https://doi.org/10.1016/j.quascirev.2012.01.005.
Wanner, H., Solomina, O., Grosjean, M., Ritz, S.P., Jetel, M., 2011. Structure and origin of Holocene cold events. Quat. Sci. Rev. 30, 3109–3123. https://doi.org/10.1016/j.quascirev.2011.07.010.
Weiss, H., 2016. Global megadrought, societal collapse and resilience at 4.2–3.9 ka BP across the Mediterranean and West Asia. PAGES 24, 62–63. https://doi.org/10.22498/pages.24.2.62.
Weldeab, S., Menke, V., Schmiedl, G., 2014. The pace of East african monsoon evolution during the Holocene. Geophys. Res. Lett. 41, 1724–1731. https://doi.org/10.1002/2014GL059361.
Wu, W., Liu, T., 2004. Possible role of the "Holocene Event 3" on the collapse of neolithic cultures around the Central Plain of China. Quat. Int. 117, 153–166. https://doi.org/10.1016/S1040-6182(03)00125-3.
Wu, W., Zheng, H., Hou, M., Ge, Q., 2018. The 5.5 cal ka BP climate event, population growth, circumscription and the emergence of the earliest complex societies in China. Sci. China Earth Sci. 61, 134–148.
Xiang, R., Sun, Y., Li, T., Oppo, D.W., Chen, M., Zheng, F., 2007. Paleoenvironmental change in the middle Okinawa Trough since the last deglaciation: evidence from the sedimentation rate and planktonic foraminiferal record. Palaeogeogr. Palaeoclimatol. Palaeoecol. 243, 378–393. https://doi.org/10.1016/j.palaeo.2006.08.016.
Xiong, H., Zong, Y., Li, T., Long, T., Huang, G., Fu, S., 2020. Coastal GIA processes revealed by the early to middle Holocene Sea-level history of East China. Quat. Sci. Rev. 233, 106249 https://doi.org/10.1016/j.quascirev.2020.106249.
Xu, F., Dou, Y., Li, J., Cai, F., Zhao, J., Wen, Z., Chen, X., Zhang, Y., Wang, L., Li, H., 2018. Low-latitude climate control on sea-surface temperatures recorded in the southern Okinawa Trough during the last 13.3 kyr. Palaeogeogr. Palaeoclimatol. Palaeoecol. 490, 210–217.
Xu, H., Yeager, K.M., Lan, J., Liu, B., Sheng, E., Zhou, X., 2015. Abrupt Holocene Indian Summer Monsoon failures: a primary response to solar activity? The Holocene 25, 677–685. https://doi.org/10.1177/0959683614566252.
Xu, Q., Meng, L., Yuan, G., Teng, F., Xin, H., Sun, X., 2020. Transgressive wave- and tide-dominated barrier-lagoon system and sea-level rise since 8.2 ka recorded in sediments in northern Bohai Bay, China. Geomorphology 352, 106978. https://doi.org/10.1016/j.geomorph.2019.106978.
Xu, Q., Xiao, J., Nakamura, T., Yang, X., Yang, Z., Liang, W., Iuchi, B., Yang, S., 2003. Quantitative reconstruction climatic changes of Daihai by pollen data. Mar. Geol. Quat. Geol. 3, 99–108 (in Chinese with English abstract).
Yu, K., Zhao, J., Liu, T., Wei, G., Wang, P., Collerson, K.D., 2004. High-frequency winter cooling and reef coral mortality during the Holocene climatic optimum. Earth Planet. Sci. Lett. 224, 143–155. https://doi.org/10.1016/j.epsl.2004.04.036.
Yu, S., Berglund, B.E., Sandgren, P., Lambeck, K., 2007. Evidence for a rapid sea-level rise 7600 yr ago. Geology 35, 891–894. https://doi.org/10.1130/G23859A.1.
Zdanowicz, C.M., Zielinski, G.A., Germani, M.S., 1999. Mount Mazama eruption: Calendrical age verified and atmospheric impact assessed. Geology 27, 621–624. https://doi.org/10.1130/0091-7613(1999)027<0621:MMECAV>2.3.CO;2.
Zhang, L., Fang, X., Ren, G., Suo, X., 1997. Environmental changes in the North China farming-grazing transitional zone. Earth Front. 4, 127–136 (in Chinese with English abstract).

Zhang, R., Delworth, T.L., 2005. Simulated tropical response to a substantial weakening of the Atlantic Thermohaline Circulation. J. Clim. 18, 1853–1860. https://doi.org/10.1175/JCLI3460.1.

Zhang, W., Chang, M., Yan, H., Dodson, J., Li, G., 2021. Synchronous changes in the East Asian-australian summer monsoons around 7.2 ka. Palaeogeogr. Palaeoclimatol. Palaeoecol. 567, 110303 https://doi.org/10.1016/j.palaeo.2021.110303.

Zhang, Z., Leduc, G., Sachs, J.P., 2014. El Niño evolution during the Holocene revealed by a biomarker rain gauge in the Galápagos Islands. Earth Planet. Sci. Lett. 404, 420–434. https://doi.org/10.1016/j.epsl.2014.07.013.

Zhao, C., Yu, Z., Ito, E., Zhao, Y., 2010. Holocene climate trend, variability, and shift documented by lacustrine stable isotope record in the northeastern United States. Quat. Sci. Rev. 29, 1831–1843. https://doi.org/10.1016/j.quascirev.2010.03.018.

Zhao, J., Li, J., Cai, F., et al., 2015. Sea surface temperature variation during the last deglaciation in the southern Okinawa Trough: Modulation of high latitude teleconnections and the Kuroshio Current. Prog. Oceanogr. 138, 238–248.

Zhao, L., Ma, C., Wen, Z., Ye, W., Shang, G., Tang, L., 2022. Vegetation dynamics and their response to Holocene climate change derived from multi-proxy records from Wangdongyang peat bog in Southeast China. Veget. Hist. Archaeobot. 31, 247–260. https://doi.org/10.1007/s00334-021-00852-z.

Zhao, L., Ma, C., Xu, Q., Deng, Y., Shang, G., Tang, L., 2021. Vegetation evolution in response to climate change and rapid sea-level rise during 8.2–7.0 cal ka BP: Pollen evidence from the northwest coast of Bohai Bay, North China. Catena 196, 104869. https://doi.org/10.1016/j.catena.2020.104869.

Zheng, X., Li, A., Kao, S., Gong, X., Frank, M., Kuhn, G., Cai, W., Yan, H., Wan, S., Zhang, H., Jiang, F., Hathorne, E., Chen, Z., Hu, B., 2016. Synchronicity of Kuroshio current and climate system variability since the last Glacial Maximum. Earth Planet. Sci. Lett. 452, 247–257. https://doi.org/10.1016/j.epsl.2016.07.028.

Zielhofer, C., Fletcher, W.J., Mischke, S., Batist, M.D., Campbell, J.F., Joannin, S., Tjallingii, K., Hamouti, N.E., Junginger, A., Stele, A., Bussmann, J., Schneider, B., Lauer, T., Spitzer, K., Strupler, M., Brachert, T., Mikdad, A., 2017a. Atlantic forcing of Western Mediterranean winter rain minima during the last 12,000 years. Quat. Sci. Rev. 157, 29–51. https://doi.org/10.1016/j.quascirev.2016.11.037.

Zielhofer, C., von Suchodoletz, H., Fletcher, W.J., Schneider, B., Dietze, E., Schlegel, M., Schepanski, K., Weninger, B., Mischke, S., Mikdad, A., 2017b. Millennial-scale fluctuations in Saharan dust supply across the decline of the African Humid Period. Quat. Sci. Rev. 171, 119–135. https://doi.org/10.1016/j.quascirev.2017.07.010.

Zielinski, G.A., Mayewski, P.A., Meeker, L.D., Whitlow, S., Twickler, M.S., 1996. A 110,000-Yr Record of explosive volcanism from the GISP2 (Greenland) ice core. Quat. Res. 45, 109–118. https://doi.org/10.1006/qres.1996.0013.

Zong, Y., Chen, Z., Innes, J.B., Chen, C., Wang, Z., Wang, H., 2007. Fire and flood management of coastal swamp enabled first rice paddy cultivation in East China. Nature 449, 459–462. https://doi.org/10.1038/nature06135.

Zong, Y., Wang, Z., Innes, J.B., Chen, Z., 2012. Holocene environmental change and Neolithic rice agriculture in the lower Yangtze region of China: a review. The Holocene 22, 623–635. https://doi.org/10.1177/0959683611409775.

Zuo, X., Lu, H., Li, Z., Song, B., 2021. Phytolith reconstruction of early to mid-Holocene vegetation and climatic changes in the lower Yangtze Valley. Catena 207, 105586. https://doi.org/10.1016/j.catena.2021.105586.